

Above-ground biomass mapping in West African dryland forest using Sentinel-1 and 2 datasets - A case study



Gerald Forkuor^{a,*}, Jean-Bosco Benewinde Zoungrana^{a,1}, Kangbeni Dimobe^{a,1}, Boris Ouattara^a, Krishna Prasad Vadrevu^b, Jérôme Ebagnerin Tondoh^c

^a West African Science Service Center on Climate Change and Adapted Land Use, Competence Center, Avenue Muamar Ghadhafi, Ouagadougou, BP 9507, Burkina Faso

^b NASA Marshall Space Flight Center, Huntsville, Alabama, USA

^c Nangui Abrogoua University, Department of Natural Sciences, 02 BP 801 Abidjan 02, Côte d'Ivoire

ARTICLE INFO

Keywords:
 Sentinel
 Above-ground biomass
 SDGs
 Random forest
 Sudanian savanna
 West africa

ABSTRACT

The Sudanian Savanna (SS) of West Africa is characterized by tropical savannas and woodlands. Accurate estimation of AGB and carbon stocks in this biome is important for addressing sustainable development goals as the information can aid natural resource management at varied spatial scales. Previous AGB mapping efforts focused on humid forests, with little attention on savannas. This study explored the use of annual monthly time-series of Sentinel-1 (S-1) and Sentinel-2 (S-2) data to map AGB in the SS. Backscatter, spectral reflectance, and derivatives (vegetation indices and biophysical parameters) were combined with field inventory data in a Random Forest regression to map AGB. Eight experiments were conducted with different data configurations to determine: (1) the potential of S-1 and S-2 for AGB mapping, (2) optimal image acquisition period for AGB mapping, and (3) contribution of image derivatives to improving the accuracy of AGB mapping. The predicted map was validated with 40% of the inventory data. Uncertainty in the AGB was assessed using mean absolute error, root mean squared error, coefficient of determination and symmetrical mean absolute percentage error. Results show that about 90% of the study area have low AGB stocks of less than 90 Mg/ha. Compared to S-1 (RMSE: 78.6; MAE: 25.6), S-2 achieved better prediction accuracy (RMSE: 60.6; MAE: 19.2), although combination of the two according to seasonality produced the best results (RMSE: 45.4; MAE: 16.3). Images acquired in the dry season were found to be more useful for predicting AGB than those of rainy season. Also, stress-related vegetation indices and a red-edge dependent normalized difference vegetation index not tested in previous AGB studies using Sentinels were found to be significant contributors to the superior performance of S-2. Since biomass is a finite resource, our results can provide valuable information on the sustainable use of biomass and energy security including studies on carbon cycling and ecosystem functions in the region. The demonstrated possibility of using open access earth observation data to map and monitor AGB in data scarce regions is useful and beneficial to attaining SDG indicators 15.2.1 (sustainable forest management) and 15.3.1 (proportion of land that is degraded over total land area). Further work on developing species-specific wood densities and allometric equations is required to improve AGB and carbon stock estimation in the SS.

1. Introduction

West Africa has been identified as a climate change hotspot where an increased probability of hazards, vulnerability, and exposure meet (Heubens et al., 2013; Sylla et al., 2015). Climate change and variability (CCV) and its effects are inducing significant land use/land cover (LULC) changes in the sub-region, resulting in unprecedented deforestation rates, degradation of arable lands and deterioration of

ecological systems (Zoungrana et al., 2018). These challenges call for appropriate adaptation and mitigation strategies to reduce the adverse effects of CCV on the sub-region's socio-ecological systems. Several global programs have been established to tackle the effects of CCV at varying scales.

The United Nations Sustainable Development Goals (SDGs) aim to, among other things, protect, restore and promote sustainable use of terrestrial ecosystems by ensuring sustainable management of forests

* Corresponding author.

E-mail addresses: forkuor.g@wascal.org (G. Forkuor), zoungrana.b@wascal.org (J.-B. Benewinde Zoungrana), dimobe.k@wascal.org (K. Dimobe), ouattara.b@edu.wascal.org (B. Ouattara), krishna.p.vadrevu@nasa.gov (K.P. Vadrevu), tondoh.e@outlook.com (J.E. Tondoh).

¹ These authors contributed equally to this work.

and reverse land degradation (SDG 15). Monitoring the spatio-temporal changes in biomass and carbon stocks is essential for the realization of several SDGs and global programs such as Reducing Emissions from Deforestation and Forest Degradation (REDD+) (Herold et al., 2011; Saatchi et al., 2011). Above and below ground biomass stocks are important sub-indicators for achieving land degradation neutrality target (15.3.1) (UNEP/CBD/SBSTTA, 2016) and sustainable forest management (FAO, 2017). Consequently, determination and monitoring of carbon stocks in forests and other land uses are important for reducing the effects of CCV and achieving sustainable development in the sub-region (Asner et al., 2013; Skutsch and Ba, 2010).

Remote Sensing (RS) data are suitable for mapping the spatial distribution of above-ground biomass (AGB) or carbon stocks over large areas. Previous mapping efforts at the scale of Africa mostly used coarse spatial resolution RS imagery (ca. 0.5 to 1 km) with limited ground reference data (Avitabile et al., 2016; Baccini et al., 2012; Dobos et al., 2001; Baccini et al., 2008). Few studies recently used relatively high resolution (30 m) optical (Baccini et al., 2017) and Synthetic Aperture Radar (SAR) data (25 m) (Bouvet et al., 2018) for large scale mapping. Despite these improvements, existing products/maps give conflicting and inconsistent AGB estimates, especially for the savanna and woodland regions of dry forests (Bouvet et al., 2018). The fragmented and heterogeneous nature of tropical dry forest areas require further efforts by way of data and methodological approaches to improve AGB estimation. Exploring the complementary use of higher resolution optical and SAR data, and incorporating significant and representative field inventory data, can enhance the accuracy and consistency of AGB estimation in tropical dry forests.

The Copernicus program of the European Commission (Moreno et al., 2012) provides open access high resolution optical (Sentinel-2, S-2) (Drusch et al., 2012) and SAR (Sentinel-1, S-1) (Torres et al., 2012) data for terrestrial research applications. Recent studies have explored these datasets, singularly or complementarily, to map forest AGB stocks in a variety of biomes. Chen et al. (2018) used S-1, S-2 and their derivatives (e.g. texture, spectral indices, biophysical variables) to map forest AGB in Jilin Province, northeast China. One parametric (Geographically weighted regression, GWR) and three non-parametric machine learning algorithms (Support Vector Machines for Regression, SVR; Random Forest, RF and Artificial Neural Networks, ANN) were compared in modeling AGB. They found both datasets to be suitable for forest AGB estimation, especially textural properties from S-1 and biophysical variables from S-2. SVR outperformed the other tested algorithms. A similar study by (L. Chen et al., 2019), which combined S-1, S-2 and elevation data from the Shuttle Radar Topographic Mission (SRTM), further emphasized the suitability of S-1 and S-2 for forest AGB mapping. However, they found RF to have outperformed GWR, SVR, ANN and linear multiple regression. Pandit et al. (2018) applied S-2 data and derived spectral indices to map AGB in sub-tropical buffer zone community forests in Nepal using RF algorithm. They found that compared to the use of only spectral bands, the inclusion of vegetation indices improved AGB prediction accuracy. The study noted the possible contribution of red-edge derived vegetation indices in enhancing the performance of the regression. An integration of Unmanned Aerial Vehicle (UAV) data, S-1 and S-2 was performed by Navarro et al. (2019) to map AGB in a mangrove plantation in Senegal. Results of a UAV-based field AGB estimation procedure (response) were regressed against predictors from S-1 (VH backscatter) and S-2 (spectral bands and vegetation indices) to predict AGB values for the entire study area. SVR was selected for the modelling and prediction. Comparison of the models using the Akaike information criterion (AIC) showed S-1 to perform better than S-2, although a combination of the two datasets produced the best results. The study further revealed that the spectral indices from S-2 were more important than spectral bands in AGB estimation. Other studies that used S-1 and/or S-2 affirmed their suitability for AGB estimation (Y. Chen et al., 2019; Haywood et al., 2018; Jay Labadisos Argamosa et al., 2018).

This study seeks to contribute to the existing knowledge on the suitability of S-1, S-2 and their derivatives for AGB mapping in the tropical dry forest of the Sudanian Savanna (SS) agro-ecological zone of West Africa. Four main vegetation types are considered – agroforestry parklands, shrub savannas, woodland/tree savannas and forest. Previous efforts at AGB estimation in sub-Saharan Africa focused on tropical humid forest areas (Akindele and LeMay 2006; Bakayoko et al., 2012; Lindsell and Klop, 2013) due to their high carbon storage potential (193–200 tons carbon/ha). On the other hand, dry forests and their associated vegetation types, estimated to have carbon storage potential of 17–70 tons carbon/ha have received less attention (Gibbs et al., 2007; Skutsch and Ba, 2010). But there are several reasons why tropical dry forests can no longer be neglected in terms of improving AGB estimation and understanding its dynamics: (1) their estimated coverage of about 22% of Africa's land area (Simons et al., 2001), (2) widespread degradation from high population growth vis-à-vis scarce resources (Campbell et al., 2007) and (3) the signing on of most countries in this biome to the REDD+ program and international conventions such as the Paris Agreement (Skutsch and Ba, 2010).

To improve biomass and carbon stock estimation in the tropical dry forest regions of the SS in West Africa, we utilized high resolution multi-temporal optical (S-2, Landsat 8) and annual monthly time-series SAR (S-1) data together with a comprehensive field dataset of inventory plots to map AGB stocks (White, 1986). S-1 and S-2 were selected because they are new, open access and have superior spatial, spectral and temporal resolution compared to other open access datasets. Landsat 8 (L-8) data were used to fill-in areas that S-2 data were not available. RF (Breiman, 2001), a machine learning non-parametric algorithm, was used for modeling AGB. Previous studies have confirmed the superior performance of non-parametric machine learning algorithms (MLA) (e.g. ANN, SVR, RF) over parametric algorithms (GWR, linear regression) (Chen et al., 2018; Wållinder, 2014). This is mainly due to the ability of the former to handle complex non-linear relationships between variables from multi-source data. However, comparisons between MLAs in estimating forest AGB and other terrestrial properties (e.g. soil) have been mostly inconclusive. For example, whereas Chen et al. (2018) found SVR to outperform RF and ANN in forest AGB estimation, Chen et al. (2019) found RF to outperform SVR and ANN in a similar study. In addition, MLA comparative studies that tested for significance found the differences between them to be minimal and statistically insignificant (Adam et al., 2014; Freeman et al., 2016). These notwithstanding, RF was selected in this study due to the relative ease of tuning, robustness against noise and its inherent ability to extract variable importance measures.

Apart from testing the suitability of S-1 and S-2 for AGB mapping in the SS, this study advances the knowledge in AGB estimation using multi-sensor satellite data in three unique ways. First, we investigated the optimal image acquisition period (within a year) for AGB estimation by analyzing annual multi-temporal (monthly) time-series of S-1 and S-2. This knowledge can reduce image processing efforts in future mapping exercises as well as financial burden of image acquisition if commercial sensors are to be used. Second, we demonstrated the complementary use of S-1 and S-2 according to rainfall seasons in the SS. Specifically, experiments were set up to determine the optimal combination of S-1 and S-2 data for improved AGB mapping. Third, a red-edge dependent index and stress-related vegetation indices (Thenkabail et al., 1994) that have not been tested with S-1/S-2 data in recent AGB estimation studies were used. To our knowledge, no study has tested S-1 and S-2 data for AGB mapping in the SS biome. Thus, we focused on the following objectives: (1) determine the potential of S-1 and S-2, individually and in combination, to map AGB in the SS agro-ecological zone of West Africa, (2) determine optimal image acquisition period for AGB modelling and (3) investigate the contribution of derivatives (e.g. indices and biophysical parameters), to AGB mapping, and (4) establish the importance of accurate AGB maps to achieving targeted indicators in the SDGs.

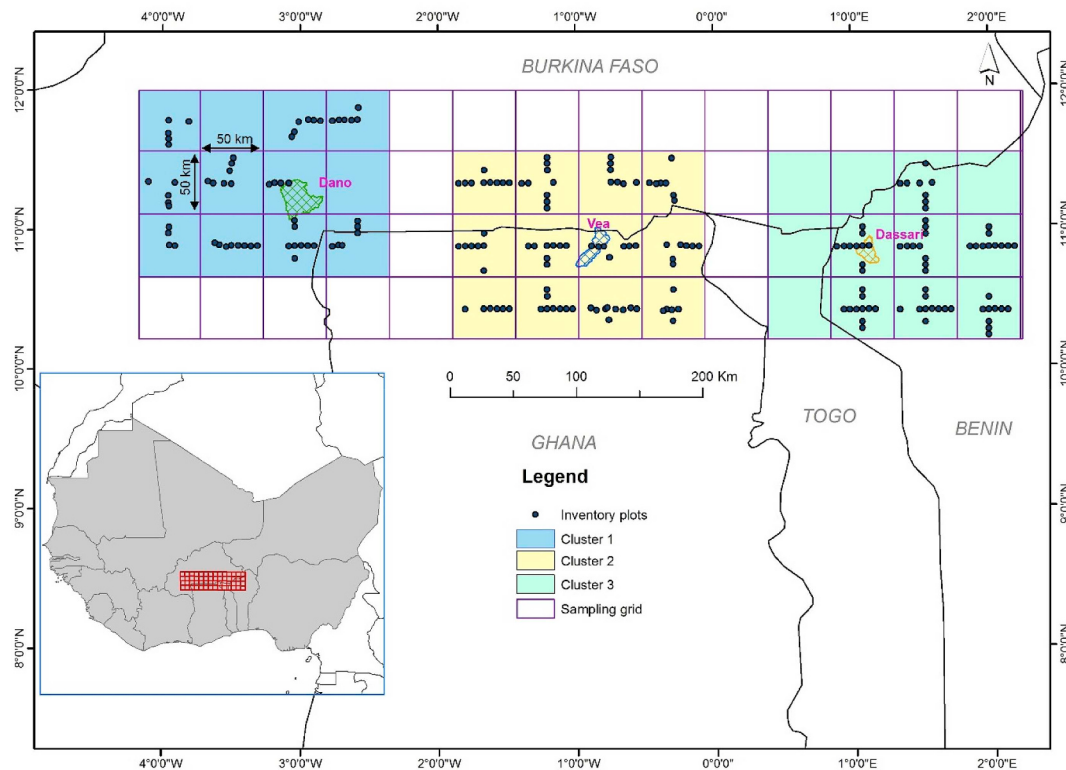


Fig. 1. Location of the study area in West Africa. The black dots indicate the spatial distribution of plots from where vegetation data were collected.

2. Materials and methods

2.1. Study area

The study was conducted in a 170,000 km² area in the SS agro-climatic region of West Africa (Fig. 1). The area covers parts of Burkina Faso, Ghana, Togo and Benin, and represents almost the combined total area of Benin (114,763 km²) and Togo (56,785 km²). These countries have all signed up to the UN-REDD + program and are at different stages of program implementation (Isyaku et al., 2017; Lund et al., 2017). They are additionally signatories to the Paris Agreement and the UN SDGs. Improving the estimation of biomass stocks through open access RS data is therefore critical for these countries.

Climatically, the study area is characterized by a mono-modal (single peak) rainfall distribution and high temperatures. Average temperature ranges from 24 °C in the southern part of the zone to about 32 °C in the north (Callo-Concha et al., 2012). Total annual rainfall ranges between 800 and 1200 mm, although this is highly variable in space and time (inter and intra-annual) (Ingram et al., 2002; Nicholson and Palao, 1993; Yilma, 2006). Typically, rainfall lasts for about 6 months from May to October during which major agricultural activities are undertaken (Callo-Concha et al., 2012). The rainy season is followed by a long dry season between November and April, during which agricultural activities cease, except isolated cases of small-scale informal irrigation (Fowe et al., 2015; Leemhuis et al., 2009).

The major vegetation types in the study area are tree (woodland) and shrub savannas with a grass layer dominated by annual grasses such as *Andropogon pseudapricus* Stapf. and *Loudetia togoensis* (Pilger) C.E. Hubbard, as well as the perennials such as *Andropogon gayanus* Kunth. and *Andropogon ascinodis* C.B.Cl (Dimobe et al., 2018a). With agriculture (crop farming and livestock rearing) as the main source of livelihood (Ghana Statistical Service, 2007; Sanfo, 2010; Sissoko et al., 2011), farmers resort to agroforestry practice, where useful tree species such as shea, baobab, locust-bean tree and others are left on farms to improve vegetation cover and partly for economic gains. Forest cover is

sparse and relatively small compared to woodlands, shrub savannas and agroforestry parklands.

Several characteristics of the SS zone can influence the intra- and inter-annual dynamics of carbon stock within the zone. First, in contrast to the evergreen tropical rainforest, the vegetation in the SS are predominantly deciduous, losing their leaves during the dry season (Hall and Swaine, 2013). Additionally, bush fires, which frequently occur during the dry season, further reduce available foliage. Biomass or carbon stocks for dry season months can therefore significantly differ from that of the rainy season for the same area. Secondly, like most of West Africa, the rainfall regime influences the vegetation types within the zone. Consequently, two (sub-) regions are often distinguished in the SS as (1) the Sudano-Guinean, a sub-humid region in the south of the zone with favorable climatic conditions and therefore higher vegetation cover/density and (2) the Sahelo-Sudanian, which is a semi-arid region in the northern part of the zone with less favorable climatic conditions and lower vegetation cover/density [33] (Fig. 1). This could potentially cause a gradient in carbon stocks within the zone.

2.2. Data acquisition and pre-processing

Three satellite image types and forest inventory data were used in this study. Details of the data source, pre-processing and extraction of variables/indices are provided in section 2.2.1.

2.2.1. Satellite images

Data from the Copernicus mission satellites S-1 and S-2 were the main satellite images used in the analysis. The two image types were combined due to their complementarity (Malenovský et al., 2012). Owing to the near independence of radar systems to weather conditions, the S-1 satellite is able to acquire usable images in excessive cloud cover conditions, a period when optical systems (S-2) fail to provide useful data. Consequently, the combined use of images from the two sensors can provide full annual image coverage for improved analysis. In addition, SAR data have been noted to have a high potential for AGB

Table 1

List of S-1 and S-2 predictors used for AGB modeling.

Sensor		Bands, indices or parameters	Definition
Sentinel-1 (monthly: January to December 2017)	Polarization	VV VH	Vertical transmit-vertical channel Vertical transmit-horizontal channel
	Indices	VH-VV (Laurin et al., 2018) VH + VV (Laurin et al., 2018)	Quotient Product
Sentinel-2 (January, February, March, November, December)	Multispectral Bands	Band 2 Band 3 Band 4 Band 5 Band 6 Band 7 Band 8 Band 8A Band 11 Band 12	Blue, 490 nm Green, 560 nm Red, 665 nm Red edge, 705 nm Red edge, 749 nm Red edge, 783 nm Near Infrared (NIR), 842 nm Near Infrared (NIR), 865 nm SWIR-1, 1610 nm SWIR-2, 2190 nm
	Vegetation Indices	NDVI (Rouse et al., 1974) NDVI _{RE} (Own construct) STVI1 (Thenkabail et al., 1994) STVI2 (Thenkabail et al., 1994) STVI3 (Thenkabail et al., 1994)	(Band 8-Band 4)/(Band 8 + Band 4) (Band 6-Band 4)/(Band 6 + Band 4) (Band 11*Band 4)/Band 8 Band 8/(Band 4*Band 12) Band 8/(Band 4*Band 11)
	Vegetation Biophysical Variables	LAI FCOVER FAPAR	Leaf Area Index Fraction of Vegetation Cover Fraction of Absorbed Photo-synthetically Active Radiation

mapping and carbon stock estimation due to the relationship between SAR backscatter and biomass (Bouvet et al., 2018; Le Toan et al., 1992). However, previous studies on AGB have mostly utilized longer wavelength SAR data such as P- and L-bands (Bouvet et al., 2018; Le Toan et al., 1992; Wingate et al., 2018) while C- and X-bands are relatively less investigated. Exploring the potential of new and largely untested SAR systems such as S-1 (Laurin et al., 2018) in mapping biomass and carbon stocks is thus essential. In instances where S-2 couldn't provide full coverage for the study area, L-8 imagery acquired for the same period was used to fill the gap. L-8 data were downloaded from the GLOVIS portal (<https://glovis.usgs.gov/>). Figure s1 depicts areas of the respective S-2 time-series that were filled with L-8 data.

S-1 data and pre-processing: S-1 data for the period January to December 2017 were downloaded from the Sentinel data hub (<https://scihub.copernicus.eu/dhus/#/home>). The data were acquired in the Interferometric Wide Swath (IW) mode with dual polarization (VV, VH). The product type was the Multi-Look Ground Range-Detected (GRD). The acquisition incidence angle ranged from 30 deg to 46 deg. A total of eleven or twelve scenes (depending on the month) covering the study area were mosaicked and subsetted for subsequent analysis. Two pre-processing procedures were applied to each scene prior to mosaicking. These are terrain correction (with radiometric normalization) and speckle filtering. ESA's Sentinel Applications Platform (SNAP) software was used for the pre-processing. The Range-Doppler Terrain Correction (RDTc) (Small and Schubert, 2008) module of SNAP was used for the terrain correction. Shuttle Radar Topographic Mission (SRTM) Digital Elevation Model (DEM) at 30 m resolution was used. The backscatter intensities of the dual polarization bands were converted to sigma nought by applying radiometric normalization. The Refined Lee speckle filtering algorithm (Lee and Pottier, 2009) was subsequently applied to the terrain and radiometrically corrected images to reduce speckle. Refined Lee was selected due to its reported superior performance when compared with other filters in SNAP (Lukin et al., 2018). The backscatter values were eventually converted to decibels using equation (1).

$$\sigma_0 (\text{dB}) = 10 \log_{10} \sigma_0 \quad (1)$$

where σ_0 dB is the normalized radar cross section and σ_0 is the

backscatter for a specific polarization.

In addition to the backscatter values, the difference (VH-VV) and sum (VH + VV) of the respective polarization bands (VH, VV) for each month were computed. Laurin et al. (2018) suggest that with backscatter values expressed in dB scale, the computed difference corresponds to a quotient while the sum can be considered as a product.

S-2 data and pre-processing: S-2 data were downloaded for the months of January, February, March, November and December 2017 from the Sentinel data hub (see Table s1 for acquisition dates). Images for the other months were not available due to excessive cloud cover for a significant part of the study area. A total of twelve 100 × 100 km S-2 tiles covered the study area. For each tile, an atmospheric correction was performed using the Sen2cor plugin in SNAP to convert the L1C (top of atmosphere) product to L2A (bottom of atmosphere) (Louis et al., 2016). Ten, out of the thirteen bands of S-2 (4 visible, 4 red edge, 2 short-wavelength infrared (SWIR)), were extracted for subsequent pre-processing and analysis. The 20 m bands of S-2 (SWIR and red edge bands) were resampled to 10 m spatial resolution using the nearest neighbor method, and all the tiles were subsequently mosaicked. Three biophysical parameters – leaf area index (LAI), fractional vegetation cover (FCOVER) and fraction of photosynthetically active radiation (FAPAR) were calculated for each image using the “Biophysical Processor” in the SNAP software. These variables have been found to be useful for biomass estimation because they describe the spatial distribution of vegetation state and dynamics (Baret et al., 2013; Dahms et al., 2016). SNAP computes the variables using tested, generic algorithms based on specific radiative transfer models. The main steps involved in the computation are (1) normalization of the inputs, (2) implementation of the artificial neural network (ANN) algorithm and (3) denormalization of the output and (4) generation of quality indicator (Weiss and Baret, 2016). In addition to the biophysical variables, five spectral vegetation indices useful for biomass modeling and estimation were computed from the S-2 data. Table 1 provides a list of all variables (bands, indices and biophysical parameters) used in this study.

L-8 data and pre-processing: L-8 scenes of S-2 areas that needed to be filled (Figure s1) were downloaded and processed. Scene numbers and information in the associated metadata files were used to convert the raw digital numbers to reflectance values. The images were resampled

Table 2

Major vegetation types considered in the inventorying and their characteristics.

Vegetation Type/Characteristics	Agroforestry parklands	Tree savanna or woodlands	Shrub savanna	Forest
Area (ha)	9.5	6.7	3.4	2.2
No. of plots	95	67	34	22
No. of trees	803	1707	733	899
DBH (cm)	32.51 ± 0.97	15.51 ± 0.28	12.47 ± 0.33	13.91 ± 0.29
Height (m)	6.76 ± 0.15	7.00 ± 0.98	4.79 ± 0.29	5.71 ± 0.48
Density (stems/ha)	84.53	254.78	215.59	408.64
Richness	46	87	62	57

to 10 m resolution using the nearest neighbor method.

2.2.2. Forest inventory data

Vegetation data were collected from three clusters of sites (Fig. 1). These clusters represent WASCAL's three experimental watersheds in Burkina Faso, Ghana and Benin (Forkuor, 2014). Between these clusters, fixed spatial grids of 50 km were defined. Within each cluster, inventory plots were established randomly in the four major vegetation types encountered in the study area. These are: (1) agroforestry parklands (croplands and fallows with trees), (2) shrub savanna, (3) tree savanna/woodland and (4) forest. Table 2 details the area, number of plots, trees, and characteristics of trees inventoried in each LULC type.

Forest inventory data were collected from September to October 2017 in 218 plots for woody perennials with diameter at breast height (DBH) ≥ 5 cm. Plots measuring 1000 m² (50 m × 20 m) were used for forest inventories using standard guidelines established for inventories in semi-arid landscapes (Ouedraogo et al., 2013; Thiombiano et al., 2015). DBH of all living trees within the plot was measured at 1.3 m above the ground level to the nearest 0.1 cm using a diameter tape. For trees forking below 1.3 m, the diameter of all ramifications was measured and DBH determined at the (quadratic mean diameter) square root of the sum of squares of individual stems. Tree height was measured from the base to the highest tip of the tree to the nearest 0.1 m using a clinometer. The 218 plots were distributed proportionally to the area of each vegetation type and this resulted in 95, 22, 34 and 67 plots established in agroforestry parklands, forest, shrub savanna and tree savanna/woodland, respectively.

2.3. AGB modeling

Fig. 2 presents an overview of the methodological approach taken to model AGB in the study area.

It entailed relating the measured AGB values to the remote sensing variables, i.e. backscatter values from S-1 and spectral information from S-2 (Table 1) through regression. Studies that used optical or SAR data or their combination in AGB mapping confirmed the relationship between spectral and backscatter information on one hand and AGB on the other (Bouvet et al., 2018; Baccini et al., 2008; Le Toan et al., 1992; Vaglio Laurin et al., 2013; Wingate et al., 2018). Four main steps were followed to derive the AGB map: (1) conversion of field data into AGB and carbon stocks, (2) extraction of training and validation data for the regression analysis (3) regression analysis and (4) accuracy assessment.

2.3.1. Calculation of biomass stocks at plot scale

To estimate AGB, shrub and tree species with DBH ≥ 5 cm were considered as they contain the greater portion of AGB. We used a minimum DBH of 5 cm in order to include only those trees and shrubs that are considered in forest inventories in the region. It has been noted that trees and shrubs with a DBH ≥ 5 are vigorous enough to withstand fire and keep their top alive, allowing species identification in the field and botanical collection (Dimobe et al., 2019). Since allometric equations are not available for most of the species in the study area, AGB was estimated using the following generalized biomass estimation model (equation (2)) developed for tropical forests (Chave et al., 2014).

$$AGB_{dry} = 0.0673 * (WD * dbh^2 * H)^{0.976} \quad (2)$$

where AGB is the above-ground biomass per tree in kg per tree; H = height (m); dbh = diameter at breast height; WD = wood density (g cm⁻³).

The *getWoodDensity* function from the BIOMASS package (Réjou-Méchain et al., 2017) in R was used to assign a wood density value to each taxon using the global wood density database as a reference (Chave et al., 2014; Zanne et al., 2009). By default, this function assigns a density value to each taxon a species- or genus-level average if at least one wood density value in the same genus as the focal taxon is available in the reference database. AGB was first computed for each individual tree and summed by plot. The amount of carbon in biomass was determined by multiplying it by a factor of 0.5 (Lung and Espira, 2015).

2.3.2. Training and validation data

Training and validation data for the regression analysis were extracted by overlaying a polygon layer of the forest inventory plots on an image stack of all predictors and extracting the corresponding values. Spatial shifts between the inventory plots and pixel boundaries ranged from 0.5 to 1.8 m (in all four cardinal directions). Such plots were shifted to ensure alignment with the image pixel boundaries prior to extracting the training and validation data. A total of 138 predictors were used, comprising of 50 S-2 spectral bands (10 bands each for five images), 25 S-2 spectral indices, 15 S-2 biophysical parameters, 24 radar backscatter bands (2 bands each for 12 images) and 24 radar difference and sum bands. The calculated AGB values (see section 3.1) were appended to the extracted spectral and backscatter values. The resulting table/values were then split into 60-40% training and validation samples using the “*createDataPartition*” function in the caret package.

2.3.3. Random Forests regression (RFR)

The regression analysis was performed using the RF MLA (Breiman, 2001). It belongs to the family of ensemble MLAs that predict a response (AGB in our case) from a set of remote sensing predictors by growing a large number of decision trees (forest) and averaging the values predicted by all trees as the final result. Each tree in the forest is independently constructed using a unique bootstrap sample of the training data. RF is preferred over standard tree-based models because it is less sensitive to noise in the training data and produces more accurate predictive models. Comparative studies involving other MLAs (e.g. SVR, ANN, etc.) also showed RF as having superior performance (Forkuor et al., 2017; Inglada et al., 2015). One feature of the RF algorithm which results in improved prediction accuracy is how predictors are selected at each node split. Unlike other MLAs (e.g. bagging and bootstrapping) (Schapire et al., 1998), in which the best predictor for node splitting is determined from all available predictors, RF chooses the best split based on a randomly selected subset of all available predictors. The introduction of this randomness in the selection of best splitting predictor decreases the correlation between trees in the forest, and consequently increases accuracy (Gislason et al., 2006). RF is robust against data redundancy, nonlinearity, and is able to handle a wide range of predictors with different properties and value

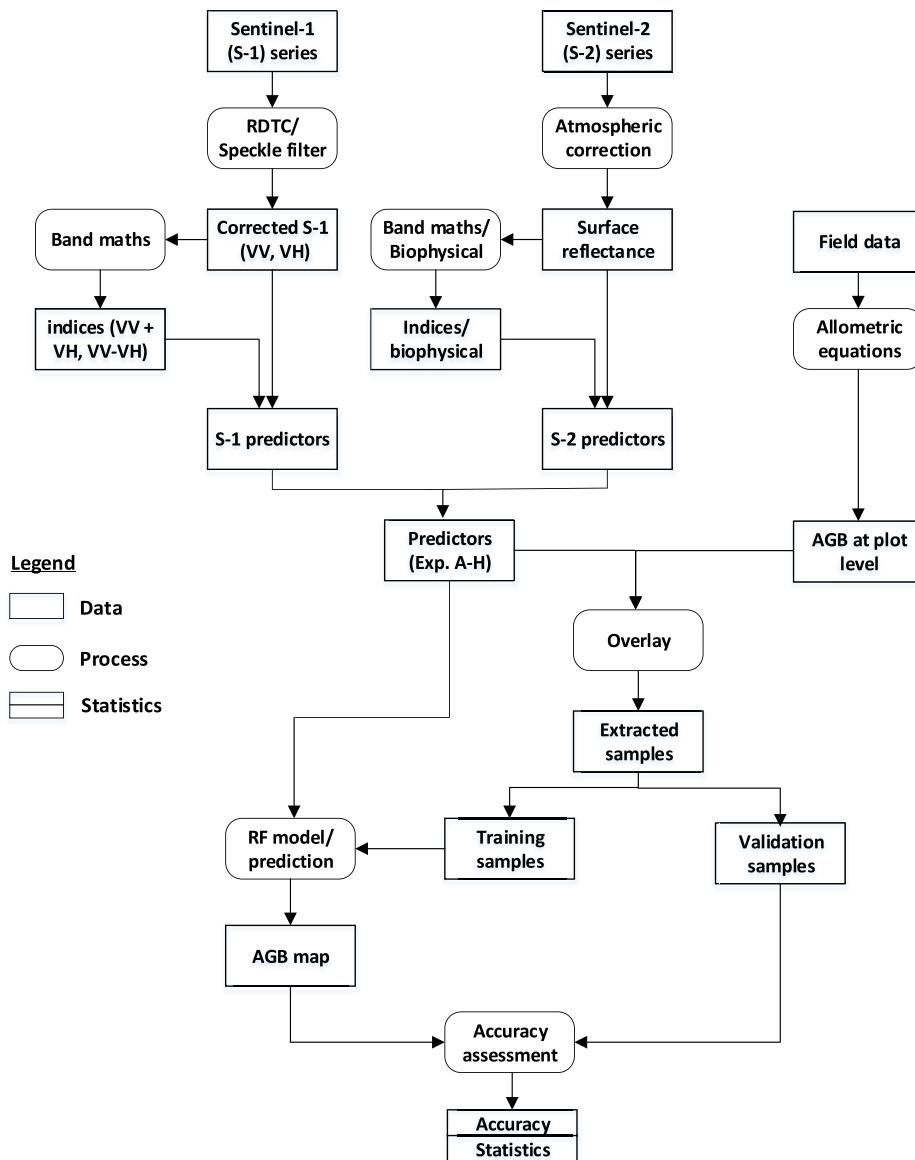


Fig. 2. Overview of methodological approach. RDTC = Range Doppler Terrain Correction.

ranges (Diaz-Uriarte and De Andres, 2006; Zhang et al., 2017). It is additionally robust against overfitting, although this may occur in instances where noisy data are being modelled (Statnikov et al., 2008). RF enables a determination of the relative importance of different predictors, which is essential for understanding the data and making future investment (financial, human) decisions in terms of data acquisition and processing.

The caret (classification and regression training) package (Kuhn et al., 2017) in the R statistical and programming environment (R Core Team, 2017) was used to implement the RFR (Kuhn et al., 2017). The caret package was chosen due to its ability to streamline the model building and evaluation process of a multitude of algorithms (Kuhn et al., 2017). The package reduces the complexity associated with model tuning by first iterating over a range of values of model parameters and selects the parameter combination that gives the best performance for building a final model. The parameters requiring tuning such as the number of trees to grow in the forest (ntree) and the number of randomly selected predictor variables at each node (mtry) were set using the grid search method in the “caret” package (Kuhn et al., 2017) and ten-fold cross validation with 5 repetitions.

2.3.3.1. Experimental design. In line with the study's objectives, eight experiments were conducted to aid in understanding the suitability of different datasets (optical, SAR, spectral, indices, biophysical, etc.) and their combinations in mapping and predicting AGB in the savanna and woodland areas of West Africa. Table 3 details the experiments and the datasets used.

2.3.4. Accuracy assessment

For each experiment, the accuracy of the prediction was assessed using the respective 40% testing data not included in the model building. Three error statistics (equations (3)–(6)) were computed in each case. These are: (1) mean absolute error (MAE), (2) root mean squared error (RMSE) and (3) symmetric mean absolute percentage error (sMAPE). It must be noted, however, that if either observed or forecasted value is negative, sMAPE (equation (5)), will return unreliable estimates (Hastie et al., 2009). In addition to the error estimates, the coefficient of determination (R^2) for each experiment was further noted (equation (6)).

$$MAE = n^{-1} \sum_{i=1}^n |P_i - O_i| \quad (3)$$

Table 3

Experimental setup in modelling above-ground biomass in the Sudanian Savanna.

Experiment	Short name	Number of predictors	Description/objective
A: All optical data	S2all	90	Spectral, indices and biophysical for five months – Jan., Feb., Mar., Nov. and Dec.
B: All SAR	S1all	48	Annual time-series plus corresponding sum and difference bands
C: Optical and SAR	S1S2all	138	All available predictors
D: S-2 spectral only	S2spe	50	Excluding indices and biophysical parameters
E: S-1 backscatter only	S1sca	24	Excluding sum and difference bands
F: S-2 biophysical	S2bio	15	Separately test the information content of these bands
G: SAR – 5 months (Jan., Feb., Mar., Nov. and Dec.)	S15mon	20	Direct comparison with optical in terms of month of acquisition
H: Annual time-series of optical and SAR	S1S2annual	118	When SAR data is used to fill-in for the months that optical sensors fail.

$$RMSE = [n^{-1} \sum_{i=1}^n (P_i - O_i)^2]^{1/2} \quad (4)$$

$$sMAPE = \frac{1}{n} \sum_{i=1}^n \frac{|O_i - P_i|}{(O_i + P_i)/2} \quad (5)$$

$$r^2 = 1 - \frac{\sum_{i=1}^n (O_i - P_i)^2}{\sum_{i=1}^n (O_i - M)^2} \quad (6)$$

where "P" is the predicted value, "O" is the observed/true value and "M" is the mean of observed values.

3. Results

3.1. AGB statistics in major vegetation types

Table 4 presents AGB statistics in the four major vegetation types considered. Shrub savannas had the least standard deviation (SD) and standard error (SE), indicating a relatively high level of uniformity within this vegetation type. Tree savanna/woodland had the highest coefficient of variation (CV) and range of AGB values, which is indicative of high variability in AGB values of plots. Mean AGB ranged from a low of 24.56 Mg/ha in shrub savanna to a high of 72.12 Mg/ha in agroforestry parklands. Woodland and forest had mean values of 28.82 and 47.66 Mg/ha, respectively..

3.2. AGB modeling with S-1, S-2 and derivatives

Table 5 presents the validation results of the eight experiments conducted with S-1 and/or S-2 images and their derivatives. Results of S2all and S1all show that multi-temporal S-2 data acquired in five months (including indices and biophysical parameters) performed better than annual monthly time-series of S-1 data in modeling AGB. This was the case for all accuracy measures computed, with an RMSE of 60.6 and 78.6 achieved for S2all and S1all respectively. In terms of sMAPE, prediction accuracies of 47% (100-sMAPE) and 31% were obtained for S2all and S1all, respectively. S15mon, which afforded a direct comparison of S-1 and S-2 in terms of months of acquisition, showed a higher RMSE of 86.6 for S1 in relation to S2. Thus, for the same months of acquisition, S-2 showed better potential in AGB modeling. Based on R², MAE, and sMAPE, modeling with the spectral bands

Table 4

AGB statistics in the major vegetation types considered.

Vegetation types	Agroforestry parklands	Tree savanna or woodland	Shrub savanna	Forest
Mean (Mg/ha)	72.12	28.82	24.56	47.66
SD	211.75	181.03	76.09	116.35
SE	7.47	4.38	2.81	3.88
CV	2.94	6.28	3.10	2.44
Range	0.01–3361.44	0.22–6574.49	0.49–1459.65	0.79–1745.92

SD = standard deviation; SE = standard error; CV = coefficient of variation.

Table 5

Validation results of the eight experiments conducted in AGB modelling.

Experiment	Validation Data			sMAPE
	RMSE	R2	MAE	
A: All optical (S2all)	60.6	0.83	19.2	0.53
B: All SAR (S1all)	78.6	0.66	25.6	0.69
C: Optical and SAR (S1S2all)	54.5	0.90	19.8	0.59
D: S-2 spectral (S2spe)	87.8	0.76	23.9	0.56
E: S-1 backscatter (S1sca)	75.4	0.76	26.1	0.67
F: S-2 biophysical (S2bio)	70.7	0.79	21.8	0.53
G: SAR – 5 months (S15mon)	86.6	0.61	28.3	0.69
H: Annual optical + SAR (S1S2annual)	45.4	0.86	16.3	0.49

of S-2 alone (S2spe) achieved better results than experiments involving all SAR data (S1all) or a subset (S15mon). Here, a prediction accuracy of 44% from only S-2 spectral bands as against 31% for annual time-series of SAR data (S1all) was realized.

3.3. Optimal predictors and image acquisition period for AGB modeling

Optimal predictors and image acquisition period for AGB modeling in the SS of West Africa were derived from the variable importance plots depicted in Fig. 3. The plots show the most important predictor variables in the eight experiments. Compared to spectral and back-scatter bands, derivatives such as red-edge dependent NDVI (NDVIR_e), FAPAR, STVI_s and the radar indices (quotient and product) were found to be better predictors of AGB. For S1S2all (all optical and SAR data combined), the most important predictor was a SAR product band (Mar.add) followed by a biophysical measure (FAPAR). Similarly, FAPAR and FCover were the first and third most important predictors in S1S2annual, in which an annual time-series of optical and SAR data were used. For experiments S2all and S1all, the first three most important variables turned out to be derivatives, further confirming the superiority of derivatives in AGB modeling in the study area. The plots further reveal that the VH polarization was mostly prominent than the VV for all experiments involving S-1 except S1sca, in which a "VV polarization" was the most important although the next four most important variables were VH polarization. In general, cross-polarizations (HV, VH) have been found to be more suitable for AGB mapping than co-polarization (HH, VV), especially at longer wavelengths (Sinha et al., 2015).

The respective variable importance plots of experiments S1S2all and S1S2annual, which included annual time-series of S-1 and S-2, were analyzed to infer the optimal periods/seasons for image acquisition in AGB mapping. The plot of experiment S1S2all reveals that all ten most important variables were acquired in the dry season (October to May). In the case of experiment S1S2annual, seven out of the ten most important variables were acquired in the dry season. Further, the plots of experiments S1all and S1sca, in which annual time-series of SAR data were used (with and without indices), also showed the importance of dry season images. Thus, compared to the rainy season, dry season images (SAR and optical) were found to be useful in predicting AGB in

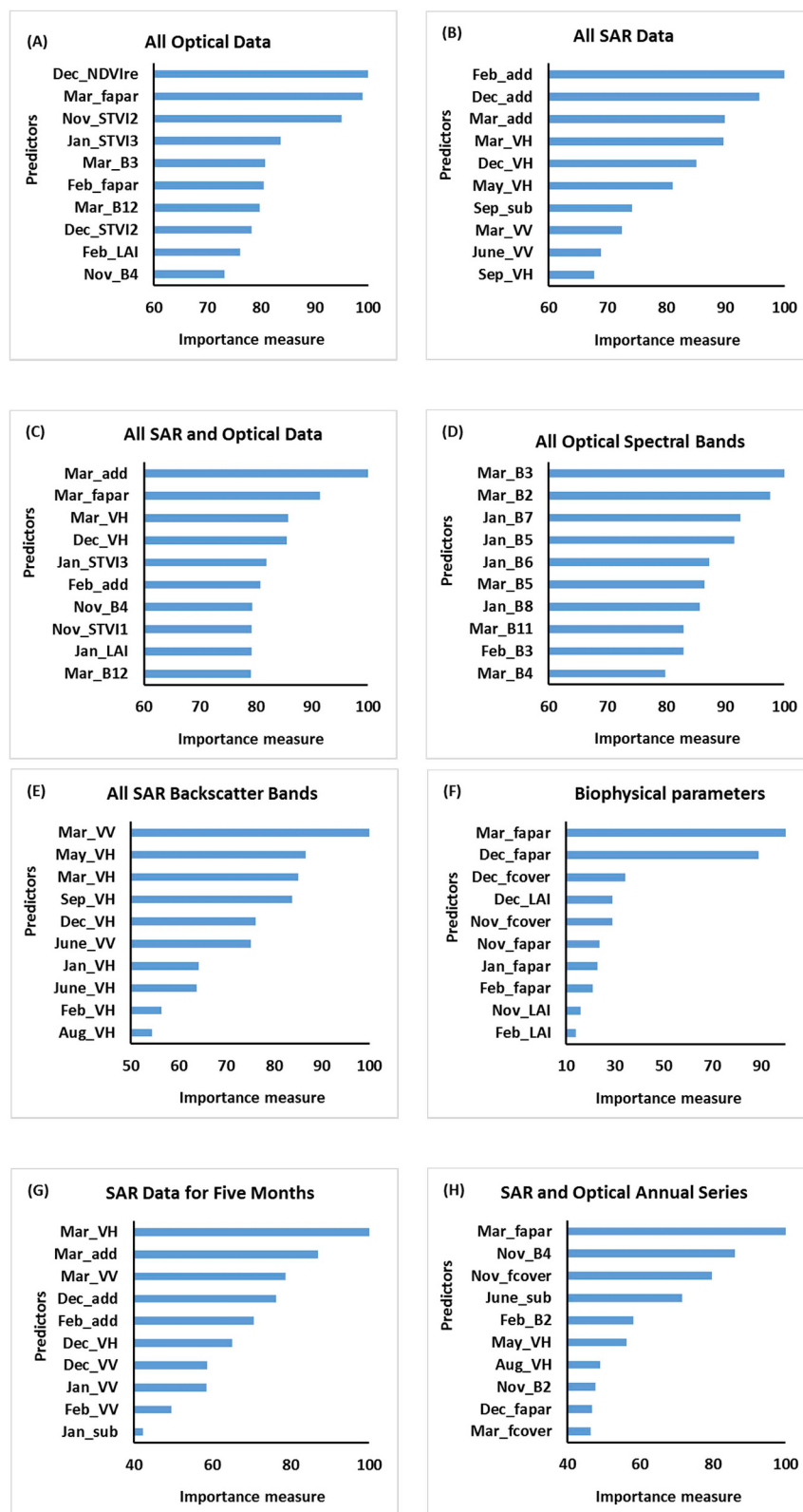


Fig. 3. Variable importance plots of the experiments conducted in AGB modelling.

the study area.

3.4. Spatial distribution of AGB

Fig. 4 shows the modelled AGB map of the study area. Water bodies were masked out of the results (white areas). AGB values range from a

low of 0.1 Mg/ha to a high of 1042 Mg/ha. However, about 90% of the study area is characterized by low AGB values ranging from 0.1 to 90 Mg/ha. The corresponding carbon stocks is 0 to 45 Mg/ha (applying a 0.5 constant). Higher AGB values are found in the east and western parts, with isolated pockets in the northern and southern portions of the study area.

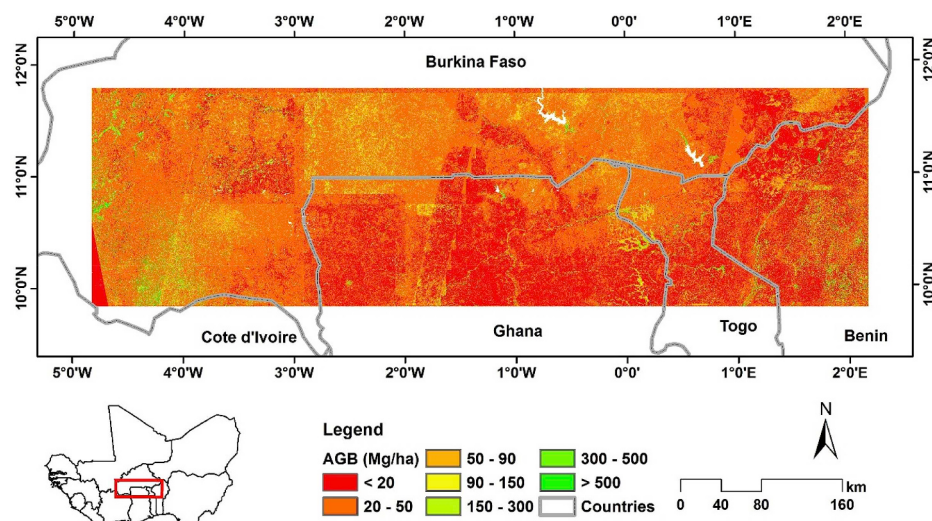


Fig. 4. Modelled AGB map of the study area. White areas represent masked out water bodies.

The modelled AGB map was compared to an existing high-resolution map (25 m) of the area developed based on ALOS PALSAR by Bouvet et al. (2018). The comparison focused on the range and distribution of AGB values in the study area (the same extent).

Fig. 5 shows that in the map developed from the current study, twenty five percent of the study area is characterized by AGB values between 0.1 and 20 Mg/ha while the corresponding value in Bouvet et al. (2018) is about 64%. Also, this study predicted almost 56% of the area to have AGB values between 20 and 50 Mg/ha compared to 26% for the same category in Bouvet et al., (2018). Both maps, however, predicted a similar percentage area for AGB value range of 50 to 90 Mg/ha. When the ranges are combined, our study and Bouvet et al., (2018) predicted 81% and 89% respectively as having AGB values between 0.1 and 50 Mg/ha. The corresponding figures for AGB values between 0.1 and 90 Mg/ha are 91% and 99% for this study and Bouvet et al., (2018), respectively. These disparities notwithstanding, the value ranges indicate that the Sudanian Savanna agroecological zone is generally characterized by low AGB values, with at least up to 90% of the studied area having AGB values less or equal to 90 Mg/ha.

We also predicted high AGB values for certain portions of the study area which may not have been captured by Bouvet et al., (2018) and other studies. We predicted nearly 8% of the study area to have AGB values greater than 90 Mg/ha compared to 0.3% by Bouvet et al., (2018). Fig. 6 shows detailed views of a S-2 RGB image acquired in November 2017 and the AGB maps produced by this study and Bouvet et al., (2018) for two extents. The first panel forms part of the Nazinga

game reserve in southern Burkina Faso. It is predominantly shrub savannas and open woodland and mostly have AGB values of between 0.1 and 50 Mg/ha. But our study predicted AGB values of between 300 and 500 Mg/ha for the gallery forest that runs through the reserve, while the map of Bouvet predicted 50 to 90 Mg/ha. Whereas 300 to 500 Mg/ha admittedly go beyond the maximum saturation value for SAR data (150 Mg/ha), the inclusion of S-2 data and associated red-edge vegetation index is expected to have reduced the effect of the saturation problem (Laurin et al., 2016; Mutanga and Skidmore, 2004; Vafaei et al., 2018).

Bouvet et al. (2018) underscored the limitation of the model-based inversion method in predicting AGB of forest plots because of forest density on radar backscatter coefficients (Mermoz et al., 2015). Therefore, some forest classes (Broadleaved evergreen closed to open forest, flooded forest, etc.) were masked out using the CCI land cover 2010 map. This could explain the obvious low AGB prediction of the dense forest areas along the river that runs through the reserve. The second panel shows a region of plantations (mainly mangoes) in southwestern Burkina Faso. Similarly, this study predicted AGB values in excess of 500 Mg/ha for closed forests and agroforestry parklands, in comparison with 50 to 90 Mg/ha by Bouvet et al. It must be noted, however, that areas with such high AGB values constitute only 1.1% of the study area.

4. Discussion

4.1. AGB in agroforestry parklands

Mean AGB values for agroforestry parklands were found to be higher than the other major vegetation types. This can be attributed to the predominance of large Vitellaria paradoxa and Parkia biglobosa tree species on most parklands. Vitellaria paradoxa provides a range of ecosystem services for rural communities and therefore has high socio-economic importance (Bayala et al., 2014; Dimobe et al., 2018b). Consequently, rural communities protect these tree species against anthropogenic effects such as excessive harvesting and pruning through farmer managed natural regeneration. Thus, compared to species in the other LULC classes, trees in agroforestry parklands have higher DBH and height (Table 2), resulting in higher AGB. Other local scale studies conducted within the study area reported relatively high mean AGBs for some of the considered vegetation types. Chabi et al. (2016) reported mean values of 94.58 ± 4.98 Mg/ha and 14.05 ± 0.72 Mg/ha, respectively for gallery forest and shrub savanna in northern Benin. Dimobe et al. (2018b) reported mean values of 147.46 ± 823.44 Mg/ha

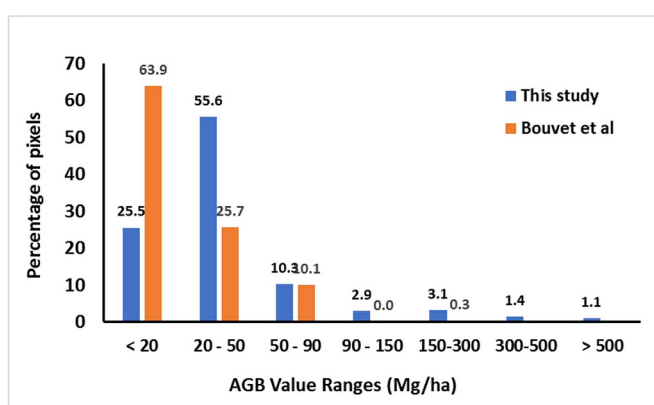


Fig. 5. Comparison of the distribution of AGB values predicted by this study and Bouvet et al. (2018).

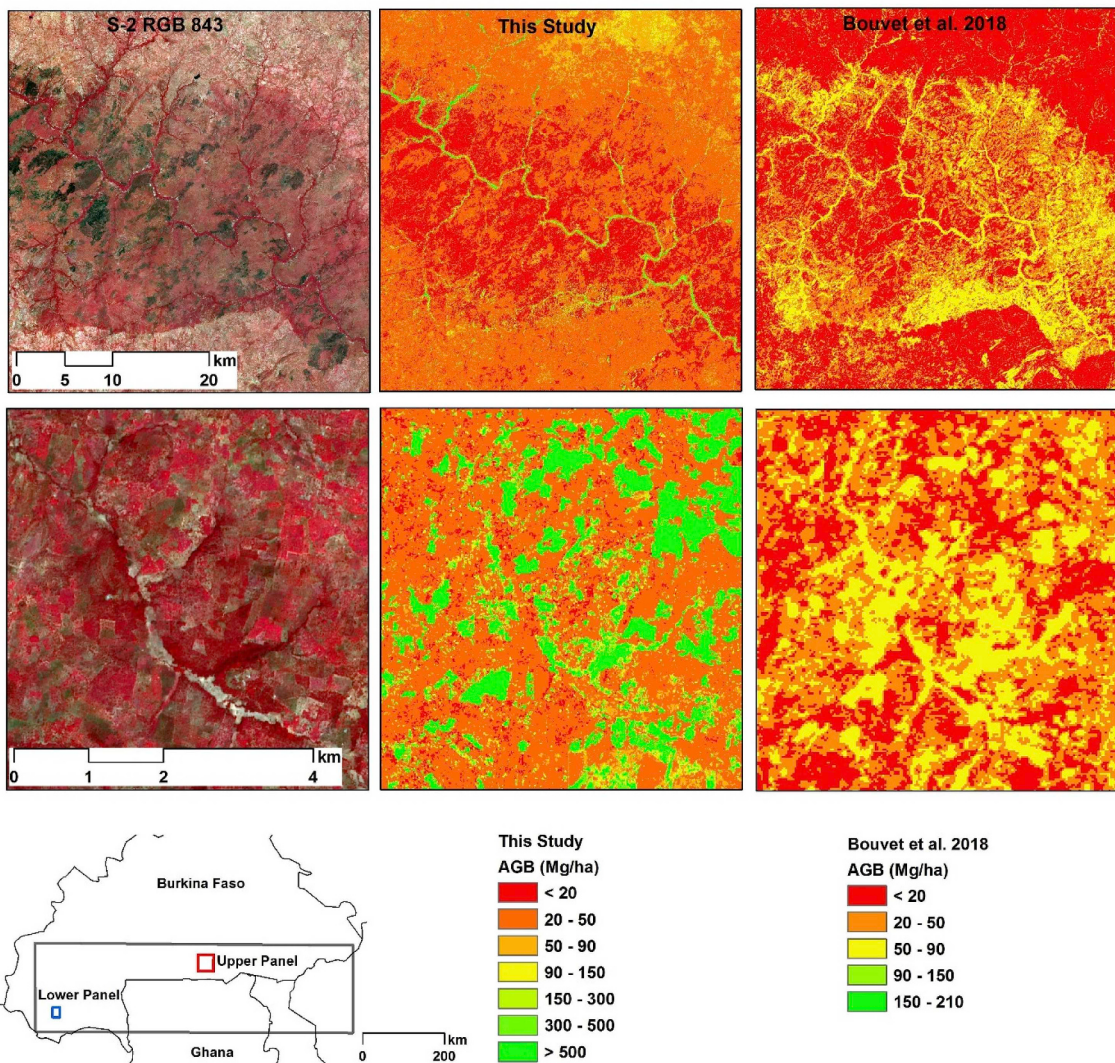


Fig. 6. Comparison between RGB 843 of Sentinel-2 image acquired in November 2018 (left), predicted AGB map by this study (middle) and predicted AGB map by Bouvet et al., (2018) (right). Upper and lower panels represent different parts of the study area (insert map). The legends apply to both panels.

ha, 123.43 ± 13.73 Mg/ha and 44.05 ± 3.23 Mg/ha for agroforestry parklands, woodlands and shrublands, respectively in Cassou (Burkina Faso). They obtained similar values in Kou (Burkina Faso). A possible reason for the relatively low mean values obtained in this study is the use of average genus and family wood density in estimating plot level AGB (see section 2.3.1), instead of species-specific values. Recent studies have shown that wood density of species within the same genus can differ greatly (Weber et al., 2018). Considering the scale of this analysis in relation to the referenced local scale studies, the use of average values from a global wood density database may have adversely affected AGB estimation at plot level.

4.2. S-1 versus S-2 for AGB modeling

The results of this study found S-2 data (optical) to be better suited for AGB modeling in the savanna woodlands of West Africa than S-1 (SAR) data. Whereas this finding agrees with some previous studies that compared optical and SAR data for AGB modeling (Vafaei et al., 2018; Zhao et al., 2016), others reported contrary results (Chen et al., 2018; Navarro et al., 2019). The performance of S-1 in this study can be attributed to two possible reasons. First, the short wavelength of S-1 (C-band) has been noted to be a limiting factor in terms of AGB modeling. Unlike longer wavelength SAR bands (e.g. L and P), C-band SAR has

limited capability to penetrate into vegetation canopy to gather the required forest structural information for improved AGB estimation. Previous research has found X- and C bands to be more sensitive to surface moisture than biomass (Pulliainen et al., 1999; Way et al., 1990), although the use of hyper-temporal time-series can enhance their sensitivity to biomass and subsequently accuracy of AGB mapping (Laurin et al., 2018; Santoro et al., 2013, 2011). Results of experiments S1all (RMSE = 78.6) and S15mon (RMSE = 86.6) indeed confirmed improved sensitivity of C-band to biomass when annual monthly S-1 time-series were used instead of a subset (5 months). A second possible reason for the performance of S-1 is the exclusion of textural information/bands in the list of predictors. Recent comparative studies that found S-1 to perform better than S-2 noted the contribution of textural information/bands in the list of predictors. This study and (Laurin et al., 2018) both found the SAR indices of quotient and product (see Table 1) to be useful for AGB modeling. Therefore, combination of this and textural information in future research should be considered for improved AGB mapping. Further, the integration of SAR data acquired from longer wavelengths (e.g. L- and P band) with S-1 and S-2 can reduce the limitation of C-band SAR and improve accuracy of AGB mapping (Laurin et al., 2018).

Despite the documented deficiency of optical data for AGB mapping,

i.e. insensitivity to biomass beyond canopy closure and interference by grasses in savannas and woodlands (Naidoo et al., 2016; Zeidler et al., 2012), S-2 data outperformed S-1 data in this study. Other studies that compared optical and SAR data for AGB modeling reported similar results. Vafaei et al. (2018), for example, compared L-band ALOS PALSAR2 and S-2 for improving AGB estimation in Iran and obtained better prediction accuracy with S-2 data (spectral bands and indices). In addition to the relatively high spatial resolution of S-2, the authors identified the inclusion of S-2 derived spectral indices and PCAs (principal component analysis) as contributing to the performance of S-2. Zhao et al. (2016) also noted that overall, Landsat TM performed better than ALOS PALSAR in estimating forest AGB in Zhejiang Province in China; however, for certain vegetation types (bamboo, Shrubland), ALOS PALSAR achieved better results.

In this study, the inclusion of S-2 derived biophysical parameters (fapar, LAI and fcover), vegetation dedicated bands such as red-edge and associated spectral indices is believed to have contributed to the performance of the S-2 data. Although previous studies have noted the usefulness of these parameters (Chen et al., 2018), experiment S2bio, and its comparison with results of other experiments, provide new insights into the importance and contribution of S-2 derived biophysical parameters to AGB modeling in the study area. The use of only biophysical parameters (15) for AGB estimation (S2bio) produced better accuracy statistics (RMSE: 70.7; R2: 0.79; MAE: 21.8; sMAPE: 0.53) than the use of all spectral bands (S2spe – 50 predictors) (RMSE: 87.8; R2: 0.76; MAE: 23.9; sMAPE: 0.56) and comparable results (RMSE: 60.6; R2: 0.83; MAE: 19.2; sMAPE = 0.53) with the use of all optical data (S2all – 90 predictors). It further outperformed all SAR (S-1) data (S1all) in AGB estimation, clearly demonstrating the advantages of biophysical parameters to AGB/carbon modeling in savanna and woodland areas.

Combining S-1 and S-2 data achieved the best results among all the experiments conducted (Table 5). Other studies that utilized S-1 and S-2 (and other optical and SAR data) in AGB estimation also found similar results (Chen et al., 2018; L. Chen et al., 2019; Laurin et al., 2018; Navarro et al., 2019; Vafaei et al., 2018). This is attributable to differences in the imaging technique, data characteristics and information content (e.g. SAR: structural information, optical: canopy density and foliage-related information) of both systems, which inure to the benefit of AGB estimation when they are combined. This knowledge notwithstanding, the use of annual monthly time-series in this study, and their combination according to climatic seasons, presents new insights into the complementarity of S-1 and S-2 for future AGB modeling exercises in data scarce regions like West Africa. Experiments S1S2all (RMSE: 54.5; R2: 0.90; MAE: 19.8; sMAPE: 0.59) and S1S2annual (RMSE: 45.4; R2: 0.86; MAE: 16.3; sMAPE = 0.49), achieved the best prediction accuracies among all the experiments. However, experiment S1S2annual, which complemented the dry season S-2 images (Jan., Feb., Mar., Nov., Dec.) with S-1 images of the remainder of the year outperformed S1S2all (all available optical and SAR images). A possible reason for this is the reduced number of S-1 data in S1S2annual, which means reduced effects of the saturation problem and general limitation of C-band SAR. Thus, for the study area, the more S-2 data available, the better for AGB modeling accuracy.

4.3. Importance of S-1 and S-2 derivatives for AGB modeling

The relative importance plots showed that in general, derivatives of S-1 and S-2 are more suitable for AGB modeling than the raw bands (spectral and backscatter) (Fig. 3). This finding was reported by other research that used S-1 and S-2 for predicting AGB. For example, Chen et al. (2018) found textural (S-1), vegetation indices and biophysical variables (S-2) to be more important than backscatter (S-1) and spectral bands (S-2) in AGB prediction. Baloloy et al. (2018) made similar observations when they used multi-spectral bands, vegetation indices and biophysical variables from Planetscope, RapidEye and S-2 to model

AGB in a forest mangrove in the Philippines. They recommended the use of S-2 derived vegetation indices rather than spectral bands. In the case of S-1, derived indices of quotient (VH-VV) and product (VH + VV) (Laurin et al., 2018) were important variables in experiments involving S-1 (e.g. S1S2all and S1S2annual). The product indices were consistently important predictors than quotient in all S-1 experiments. This is contrary to the findings of Laurin et al. (2018), who found the quotient indices of a season to be more important for AGB modeling than the product. This difference notwithstanding, both studies point to the relative importance of S-1 derivatives over backscatter bands.

With respect to S-2, testing of a red-edge dependent vegetation index (NDVI_re) and the STVIs in this study provides new information on the use of S-2 data for AGB modeling. NDVI_re was found to be the most important variable in experiment S2all (all optical bands), outperforming other vegetation indices and biophysical parameters. Compared to conventional vegetation indices (e.g. NDVI), red-edge derived vegetation indices are known to mitigate the saturation problem in biomass estimation (Laurin et al., 2016; Mutanga and Skidmore, 2004). On the other hand, the performance of the STVI2 and 3 in experiments S2all and S1S2all (Fig. 3) is quite revealing and confirms the usefulness of both near and middle infrared bands (SWIR in this case) in monitoring vegetation in semi-arid environments (Mundava et al., 2014; Thenkabail et al., 1994). Although these indices were originally defined and used in agricultural applications (Thenkabail et al., 1994), the results of this study suggest their potential use for AGB mapping in semi-arid environments. Other biomass modelling related studies conducted in semi-arid regions found STVIs as strongly correlated to perennial vegetation and total ground cover (Jafari et al., 2007; Mundava et al., 2014; O'Neill, 1996). These studies considered vegetation types such as open plains and grassland ecosystems, which are similar to shrub savannas and woodlands in our study area.

Based on the variable importance plots, this study revealed a greater contribution from FAPAR and FCOVER than LAI (i.e. was not included in the top 10 important variables in experiments S2all, S1S2all or S1S2annual). Baloloy et al. (2018) found low correlations for LAI and FCOVER in AGB prediction, while chlorophyll-a (CAB) showed relatively higher correlation. In contrast, Chen et al. (2018) found a higher correlation between LAI and AGB compared to FCOVER, CAB and FAPAR. Castillo et al. (2017) obtained a similar result when they found LAI as the most important biophysical variable for predicting AGB in a mangrove forest in the Philippines. These differences (compared to ours) may be due to differences in the composition and nature of vegetation being modelled. For example, Baloloy et al. (2018) attributed the relatively poor performance of LAI to the presence of undergrowth vegetation and layering in their study area. The results of Chen et al. (2018) may be due to the presence of high forest cover in their study area, in contrast to that of Baloloy et al. (2018) (mangrove plantation) and the current study (savannas and woodlands).

4.4. Effect of seasonality on data selection

The variable importance plots of experiments S1S2all and S1S2annual (with annual monthly time-series) revealed that images acquired in the dry season (October to May) are important for AGB modeling in the study area. The sensitivity of S-1 and other SAR data to seasonal variation due to changes in vegetation canopy, water content, soil moisture, etc. has been noted by other studies (Bouvet et al., 2018; Guccione et al., 2016; Vaglio Laurin et al., 2013). Although most vegetation types in the study area are expected to have higher vegetation cover during the rainy season and therefore better correlation with remotely sensed data, other factors such as vegetation water content (humid and wet canopies) and soil moisture could reduce the sensitivity of SAR data to the biomass (Nguyen et al., 2016). In the case of S-1, its relatively short wavelength and subsequent low canopy penetration

could be advantageous for landscapes with open and deciduous vegetation in which branches get exposed during the dry season (leaf-off period) (Vaglio Laurin et al., 2013). Our findings on seasonality agree with Nguyen et al. (2016), who used ALOS-2 SAR data to estimate tropical forest structural characteristics including the effect of polarization and seasonality of the SAR data on forest biomass estimation in the Yok Don National Park, Vietnam. They found that the dry season SAR backscatter intensity was highly sensitive to the AGB of forest compared to the rainy season backscatter intensity. They found the HV cross-polarization band to explain 54% variation of the biomass. This finding is highly relevant for AGB modelling in West Africa where optical sensors fail to deliver useful images during the wet season due to excessive cloud cover. Unlike agricultural applications such as crop mapping which require rainy season images (Forkuor et al., 2014), this study has shown that dry season images may be sufficient for accurate AGB modeling in the savanna regions of West Africa. Nonetheless, the integration of open access SAR data from ESA for periods when optical data are not available can enhance the modeling accuracy.

4.5. Relevance of results to SDG attainment

The UN SDGs spell out the commitment of the international community to rid the world of poverty and hunger and achieve sustainable development in its three dimensions – economic, social and environmental. The seventeen goals and associated 169 targets cover critical human and development sectors including poverty, food security, gender equality, water, energy, climate change, industrial development, and global partnerships. Apart from using comparable and standardized national official data sources as the basis for monitoring and reporting on these goals and targets, earth observation, geospatial information and global/regional datasets have been identified as viable replacement and complementary data sources for achieving the SDGs (UNEP/CBD/SBSTTA, 2016). In this regard, the objectives and subsequent results of this study are directly applicable and useful for the attainment of two targets (15.2, 15.3) under SDG 15 (“protect, restore and promote sustainable use of terrestrial ecosystems, sustainably manage forests, combat desertification, and halt and reverse land degradation and halt biodiversity loss”), although implicit links can be made to five other SDGs (2, 7, 9, 12, 13) (Müller et al., 2015).

Increasing population growth has led to high demand for forest products, unsustainable forest management practices and high deforestation rates. As an important carbon sink, unsustainable exploitation of forests causes the release of CO₂ into the atmosphere, negatively impacting the global climate cycle (Federici et al., 2015). To reduce this effect, the Inter-agency Expert Group on SDG Indicators (IAEG-SDGs) proposed an indicator to monitor progress towards sustainable forest management (SFM) (indicator 15.2.1) (UNSD, 2019). Five sub-indicators, including monitoring of *above-ground biomass stocks in forests*, have subsequently been defined to aid in monitoring the economic, social and environmental dimensions of SFM. Comparison of country-level indicator values from one year to the other enable a determination of the progress being made towards SFM. Thus, a stable or increasing biomass stock per hectare over a period will indicate SFM while a long-term reduction of biomass stock per hectare would imply either unsustainable management of the forests and degradation (FAO, 2017). The demonstrated possibility to use freely available optical and SAR data to map biomass stocks, especially in data scarce regions like West Africa, will greatly assist countries in accurately deriving, monitoring and reporting on SDG indicator 15.2.1.

Another SDG indicator that benefits from the accurate estimation and monitoring of above-ground biomass stocks is SDG indicator 15.3.1 (proportion of land that is degraded over total land area), which relies on three sub-indicators including above- and below-ground carbon stocks (the others being land cover and land cover change and land productivity). By regularly mapping these sub-indicators, countries will be able to measure and evaluate changes in each sub-indicator and be

able to monitor and showcase their efforts at combatting desertification and achieving land degradation neutrality.

5. Conclusion

This study mapped AGB in the dry forest of the SS using multi-temporal S-1, S-2, their derivatives (indices, biophysical parameters) and inventory data in a Random Forest Regression (RFR). Vegetation types considered are agroforestry parklands, shrub savannas, woodlands and forest. Eight experiments involving different combinations of the data were conducted to achieve the objectives of the study. Analysis of multi-temporal S-2 achieved better accuracy than S-1, although a complementary use of the two provided the highest accuracies. A red-edge dependent NDVI and STVs not tested in previous AGB studies using Sentinels were found to be important predictors and significant contributors to the superior performance of S-2. Compared to conventional vegetation indices (e.g. NDVI), red-edge derived vegetation indices have been reported to reduce the effect of the saturation problem in biomass estimation. The performance of the STVs was due to the occurrence of savanna-like vegetation cover in the study area. Modeling with only multi-temporal S-2-derived biophysical parameters (FAPAR, LAI, FCover) outperformed annual monthly S-1 time-series, emphasizing the importance of biophysical parameters in AGB modeling.

The findings of this study revealed the importance of using annual time-series RS data for AGB mapping in the study area. AGB modeling with annual monthly S-1 time-series achieved better accuracy than a subset (5-months), confirming previous findings that the use of hyper-temporal C-band SAR can enhance their sensitivity to biomass and increase accuracy. However, complementing S-1 and S-2 data according to seasonality (i.e., S-1: rainy season; S-2: dry season) produced the best accuracy for AGB mapping. In this regard, ESA's open access policy on the Sentinels is promising for AGB and carbon stock mapping in West Africa. The relative ease of obtaining S-2 data in the dry season and S-1 in the rainy season (due to independence of SAR systems to cloud cover) would afford such optimal combination of data for enhanced AGB mapping accuracies. Apart from using multi-temporal S-1 data, future studies may, when available, combine SAR data of longer wavelength with S-1 and S-2 to further reduce the wavelength limitation of S-1.

The predicted AGB map revealed that 90% of the study area is characterized by low AGB values (< 90 Mg/ha). Highest mean AGB value of 72.12 Mg/ha was found in agroforestry parklands. The dominant tree species in parklands (*Vitellaria paradoxa* and *Parkia biglobosa*) tend to be large due to their preservation by rural communities for economic benefit and derivation of essential ecosystem services. On the other hand, overexploitation of other vegetation types (e.g. fuel harvesting) have led to thinning of tree species, which may have contributed to the generally low AGB values observed. But, the number and distribution of reference data, the use of default wood density values and global biomass equation for AGB estimation must be improved in future studies. Further work on developing species-specific wood densities in this biome is required for improving AGB and carbon stock modeling at regional scales. Recent, less laborious and less destructive approaches to generating reference data, e.g. the use of UAVs as presented by Navarro et al. (2019) must be explored in future efforts. Although this may have an initial high cost, it will eventually inure to the benefit of routine monitoring of AGB and carbon stocks for attaining SDGs and other global programs such as REDD+.

The demonstrated possibility of using open access earth observation data to map and monitor AGB in data scarce developing countries is directly useful and beneficial to attaining SDG indicators 15.2.1 (sustainable forest management) and 15.3.1 (proportion of land that is degraded over total land area). By regularly mapping the relevant sub-indicators, countries will be able to measure and evaluate changes and showcase their efforts at attaining sustainable forest management and land degradation neutrality.

Acknowledgements

The authors are grateful to the European Space Agency and the United States Geological Survey for their open data policy. We acknowledge financial support from the German Federal Ministry of Education and Research (BMBF), Germany, under the research grant 01LG1001A.

Appendix A. Supplementary data

Supplementary data to this article can be found online at <https://doi.org/10.1016/j.rse.2019.111496>.

References

- Adam, E., Mutanga, O., Odindi, J., Abdel-Rahman, E.M., 2014. Land-use/cover classification in a heterogeneous coastal landscape using RapidEye imagery: evaluating the performance of random forest and support vector machines classifiers. *Int. J. Remote Sens.* 35, 3440–3458. <https://doi.org/10.1080/01431161.2014.903435>.
- Akindele, S.O., LeMay, V.M., 2006. Development of tree volume equations for common timber species in the tropical rain forest area of Nigeria. *For. Ecol. Manage.* 226, 41–48. <https://doi.org/10.1016/j.foreco.2006.01.022>.
- Asner, G.P., Mascaro, J., Anderson, C., Knapp, D.E., Martin, R.E., Kennedy-Bowdoin, T., van Breugel, M., Davies, S., Hall, J.S., Muller-Landau, H.C., Potvin, C., Sousa, W., Wright, J., Birmingham, E., 2013. High-fidelity national carbon mapping for resource management and REDD+. *Carbon Balance Manag.* 8, 1–14. <https://doi.org/10.1186/1750-0680-8-7>.
- Avitabile, V., Herold, M., Heuvelink, G.B.M., Lewis, S.L., Phillips, O.L., Asner, G.P., Armston, J., Ashton, P.S., Banin, L., Bayol, N., others, 2016. An integrated pan-tropical biomass map using multiple reference datasets. *Glob. Chang. Biol.* 22, 1406–1420.
- Baccini, A., Goetz, S.J., Walker, W.S., Laporte, N.T., Sun, M., Hackler, J., 2012. Estimated carbon dioxide emissions from tropical deforestation improved by carbon-density maps. *Nat. Clim. Chang.* 2, 1–4. <https://doi.org/10.1038/nclimate1354>.
- Baccini, A., Laporte, N., Goetz, S.J., Sun, M., Dong, H., 2008. A first map of tropical Africa's above-ground biomass derived from satellite imagery. *Environ. Res. Lett.* 3 (4), 45011.
- Baccini, A., Walker, W., Carvalho, L., Farina, M., Houghton, R.A., 2017. Tropical Forests Are a Net Carbon Source Based on Aboveground Measurements of Gain and Loss 5962, pp. 1–11.
- Bakayoko, O., Assa, A.M., Coulibaly, B., N'guesso, K.A., 2012. Stockage de Carbone dans des Peuplements de Cedrela Odorata et de Gmelina Arborea en Côte d'Ivoire. *Eur. J. Sci. Res.* 75, 490–501.
- Baloy, A.B., Blanco, A.C., Cândido, C.G., Argamosa, R.J.L., Dumalag, J., Dimapilis, L.L.C., Paringit, E.C., 2018. Estimation OF mangrove forest aboveground biomass using multispectral bands, vegetation indices and biophysical variables derived from optical satellite imagers: rapideye, planetscope and SENTINEL-2. *Int. Arch. Photogramm. Remote Sens. Spat. Inf. Sci.* 4.
- Baret, F., Weiss, M., Lacaze, R., Camacho, F., Makhmara, H., Pacholczyk, P., Smets, B., 2013. GEOV1: LAI and FAPAR essential climate variables and FCOVER global time series capitalizing over existing products. Part1: principles of development and production. *Remote Sens. Environ.* 137, 299–309. <https://doi.org/10.1016/j.rse.2012.12.027>.
- Bayala, J., Sanou, J., Teklehaimanot, Z., Kalinganire, A., Ouédraogo, S.J., 2014. Parklands for buffering climate risk and sustaining agricultural production in the Sahel of West Africa. *Curr. Opin. Environ. Sustain.* 6, 28–34.
- Bouvet, A., Mermoz, S., Le Toan, T., Villard, L., Mathieu, R., Naidoo, L., Asner, G.P., 2018. An above-ground biomass map of African savannahs and woodlands at 25 m resolution derived from ALOS PALSAR. *Remote Sens. Environ.* 206, 156–173. <https://doi.org/10.1016/j.rse.2017.12.030>.
- Breiman, L., 2001. Random forests. *Mach. Learn.* 45, 5–32. <https://doi.org/10.1023/A:1010933404324>.
- Callo-Concha, D., Gaiser, T., Ewert, F., 2012. Farming and Cropping Systems in the West African Sudanian Savanna (No. 100). ZEF Working Paper Series, Bonn.
- Campbell, B.M., Angelsen, A., Cunningham, A., Katerere, Y., Sitoe, A., Wunder, S., 2007. Miombo Woodlands-Opportunities and Barriers to Sustainable Forest Management. CIFOR, Bogor, Indones (4th Novemb. 2008). <http://www.cifor.cgiar.org/miombo/docs/CampbellBarriersandOpportunities.pdf>.
- Castillo, J.A.A., Apan, A.A., Maraseni, T.N., Salmo III, S.G., 2017. Estimation and mapping of above-ground biomass of mangrove forests and their replacement land uses in the Philippines using Sentinel imagery. *ISPRS J. Photogrammetry Remote Sens.* 134, 70–85.
- Chabi, A., Lautenbach, S., Orekan, V.O.A., Kyei-Baffour, N., 2016. Erratum : allometric models and aboveground biomass stocks of a West African Sudan Savannah watersheds in Benin. [Carbon Balance Manag., 11, (2016), (16)] Doi: 10.1186/s13021-016-0058-5. *Carbon Balance Manag.* 11. <https://doi.org/10.1186/s13021-016-0064-7>.
- Chave, J., Réjou-Méchain, M., Bürquez, A., Chidumayo, E., Colgan, M.S., Delitti, W.B.C., Duque, A., Eid, T., Fearnside, P.M., Goodman, R.C., Henry, M., Martínez-Yrízar, A., Mugasha, W.A., Muller-Landau, H.C., Mencuccini, M., Nelson, B.W., Ngomanda, A., Nogueira, E.M., Ortiz-Malavassi, E., Pélassier, R., Ploton, P., Ryan, C.M., Saldarriaga, J.G., Vieilledent, G., 2014. Improved allometric models to estimate the aboveground biomass of tropical trees. *Glob. Chang. Biol.* 20, 3177–3190. <https://doi.org/10.1111/gcb.12629>.
- Chen, L., Ren, C., Zhang, B., Wang, Z., Xi, Y., 2018. Estimation of forest above-ground biomass by geographically weighted regression and machine learning with sentinel imagery. *Forests* 9, 582.
- Chen, L., Wang, Y., Ren, C., Zhang, B., Wang, Z., 2019. Optimal combination of predictors and algorithms for forest above-ground biomass mapping from sentinel and SRTM data. *Remote Sens.* 11, 414. <https://doi.org/10.3390/rs11040414>.
- Chen, Y., Li, L., Lu, D., Li, D., 2019. Exploring bamboo forest aboveground biomass estimation using Sentinel-2 data. *Remote Sens.* 11, 1–22. <https://doi.org/10.3390/rs11010007>.
- Dahms, T., Seissiger, S., Borg, E., Vajen, H., Fichtelmann, B., Conrad, C., 2016. Important variables of a rapideye time series for modelling biophysical parameters of winter wheat. *Photogramm. Fernerkund. Geoinf. (PFG)* 2016, 285–299.
- Diaz-Uriarte, R., De Andres, S.A., 2006. Gene selection and classification of microarray data using random forest. *BMC Bioinf.* 7, 3.
- Dimobe, K., Kuyah, S., Dabré, Z., Ouédraogo, A., Thiombiano, A., 2019. Diversity-carbon stock relationship across vegetation types in W National park in Burkina Faso. *For. Ecol. Manage.* 438, 243–254.
- Dimobe, K., Mensah, S., Goetze, D., Ouédraogo, A., Kuyah, S., Porembski, S., Thiombiano, A., 2018a. Aboveground biomass partitioning and additive models for Combretum glutinosum and Terminalia laxiflora in West Africa. *Biomass Bioenergy* 115, 151–159. <https://doi.org/10.1016/j.biombioe.2018.04.022>.
- Dimobe, K., Tondoh, J.E., Weber, J.C., Bayala, J., Ouédraogo, K., Greenough, K., 2018b. Farmers' preferred tree species and their potential carbon stocks in southern Burkina Faso: implications for biocarbon initiatives. *PLoS One* 13, e0199488.
- Dobos, E., Montanarella, L., Nègre, T., Micheli, E., 2001. A regional scale soil mapping approach using integrated AVHRR and DEM data. *Int. J. Appl. Earth Obs. Geoinf.* 3, 30–42. [https://doi.org/10.1016/S0964-5710\(01\)80109-4](https://doi.org/10.1016/S0964-5710(01)80109-4).
- Drusch, M., Del Bello, U., Carlier, S., Colin, O., Fernandez, V., Gascon, F., Hoersch, B., Isola, C., Laberinti, P., Martimort, P., Meygret, A., Spoto, F., Sy, O., Marchese, F., Bargellini, P., 2012. Sentinel-2: ESA's optical high-resolution mission for GMES operational services. *Remote Sens. Environ.* 120, 25–36. <https://doi.org/10.1016/j.rse.2011.11.026>.
- FAO, 2017. KEEPING an EYE on SDG 15. Rome, Italy.
- Federici, S., Tubiello, F.N., Salvatore, M., Jacobs, H., Schmidhuber, J., 2015. New estimates of CO₂ forest emissions and removals: 1990–2015. *For. Ecol. Manage.* 352, 89–98.
- Forkuor, G., 2014. Agricultural Land Use Mapping in West Africa Using Multi-Sensor Satellite Imagery. University of Wuerzburg.
- Forkuor, G., Conrad, C., Thiel, M., Ullmann, T., Zoungrana, E., 2014. Integration of optical and synthetic aperture radar imagery for improving crop mapping in north-western Benin, West Africa. *Remote Sens.* 6. <https://doi.org/10.3390/rs6076472>.
- Forkuor, G., Hounkpatin, O.K.L., Welp, G., Thiel, M., 2017. High resolution mapping of soil properties using remote sensing variables in south-western Burkina Faso: a comparison of machine learning and multiple linear regression models. *PLoS One* 12, 1–21. <https://doi.org/10.1371/journal.pone.0170478>.
- Fowe, T., Karambir, H., Paturel, J.-E., Poussin, J.-C., Cecchi, P., 2015. Water balance of small reservoirs in the Volta basin: a case study of Boura reservoir in Burkina Faso. *Agric. Water Manag.* 152, 99–109. <https://doi.org/10.1016/j.agwat.2015.01.006>.
- Freeman, E.A., Moisen, G.G., Coulston, J.W., Wilson, B.T., 2016. Random forests and stochastic gradient boosting for predicting tree canopy cover: comparing tuning processes and model performance ¹. *Can. J. For. Res.* 46, 323–339. <https://doi.org/10.1139/cjfr-2014-0562>.
- Ghana Statistical Service, 2007. Pattern and Trends of Poverty in Ghana, 1991–2006. Ghana Statistical Service.
- Gibbs, H.K., Brown, S., Niles, J.O., Foley, J.A., 2007. Monitoring and estimating tropical forest carbon stocks: making REDD a reality. *Environ. Res. Lett.* 2. <https://doi.org/10.1088/1748-9326/2/4/045023>.
- Gislason, P.O., Benediktsson, J.A., Sveinsson, J.R., 2006. Random Forests for land cover classification. *Pattern Recognit. Lett.* 27, 294–300. <https://doi.org/10.1016/j.patrec.2005.08.011>.
- Guccione, P., Lombardi, A., Giordano, R., 2016. Assessment of seasonal variations of radar backscattering coefficient using Sentinel-1 data. In: Geoscience and Remote Sensing Symposium (IGARSS), 2016 IEEE International, pp. 3402–3405.
- Hall, J.B., Swaine, M.D., 2013. Distribution and Ecology of Vascular Plants in a Tropical Rain Forest: Forest Vegetation in Ghana. Springer Science & Business Media.
- Hastie, T., Tibshirani, R., Friedman, J., 2009. The elements of statistical learning: data mining, inference, and prediction, Second. Springer-Verlag, New York.
- Haywood, A., Stone, C., Jones, S., 2018. The potential of sentinel satellites for large area aboveground forest biomass mapping. In: IGARSS 2018–2018 IEEE International Geoscience and Remote Sensing Symposium, pp. 9030–9033.
- Herold, M., Román-Cuesta, R.M., Mollicone, D., Hirata, Y., Van Laake, P., Asner, G.P., Souza, C., Skutsch, M., Avitabile, V., MacDicken, K., 2011. Options for monitoring and estimating historical carbon emissions from forest degradation in the context of REDD+. *Carbon Balance Manag.* 6, 1–7. <https://doi.org/10.1186/1750-0680-6-13>.
- Heubel, J., Schmidt, M., Stuch, B., García Márquez, J.R., Wittig, R., Zizka, G., Thiombiano, A., Sinsin, B., Schaldach, R., Hahn, K., 2013. The projected impact of climate and land use change on plant diversity: an example from West Africa. *J. Arid Environ.* 96, 48–54. <https://doi.org/10.1016/j.jaridenv.2013.04.008>.
- Ingla, J., Arias, M., Tardy, B., Hagolle, O., Valero, S., Morin, D., Dedieu, G., Sepulcre, G., Bontemps, S., Defourny, P., Koetz, B., 2015. Assessment of an operational system for crop type map production using high temporal and spatial resolution satellite optical imagery. *Remote Sens.* 7, 12356–12379. <https://doi.org/10.3390/rs70912356>.

- Ingram, K.T., Roncoli, M.C., Kirshen, P.H., 2002. Opportunities and constraints for farmers of west Africa to use seasonal precipitation forecasts with Burkina Faso as a case study. *Agric. Syst.* 74, 331–349. [https://doi.org/10.1016/S0308-521X\(02\)00044-6](https://doi.org/10.1016/S0308-521X(02)00044-6).
- Iisyaku, U., Arhin, A.A., Asiyani, A.P., 2017. Framing justice in REDD+ governance: centring transparency, equity and legitimacy in readiness implementation in West Africa. *Environ. Conserv.* 44, 212–220.
- Jafari, R., Lewis, M.M., Ostendorf, B., 2007. Evaluation of vegetation indices for assessing vegetation cover in southern arid lands in South Australia. *Rangel. J.* 29, 39–49.
- Jay Labadisos Argamosa, R., Conferido Blanco, A., Balidoy Baloloy, A., Gumbao Candido, C., Barr Lovern Caboboy Dumalag, J., Lee Carandang Dlimapilis, Lady, Camero Paringit, E., 2018. MODELLING above GROUND BIOMASS of MANGROVE FOREST USING SENTINEL-1 IMAGERY. *Int. Arch. Photogramm. Remote Sens. Spat. Inf. Sci.* 4, 13–20. <https://doi.org/10.5194/isprs-analys-IV-3-13-2018>.
- Kuhn, M., Wing, J., Weston, S., Williams, A., Keefer, C., Engelhardt, A., Cooper, T., Mayer, Z., Kenkel, B., Team, the R.C., Benesty, M., Lescarbeau, R., Ziem, A., Scrucca, L., Tang, Y., Candan, C., 2017. Caret: classification and regression training. [WWW Document]. R Packag. version 6.0-76. URL <http://cran.r-project.org/package=caret>.
- Laurin, G.V., Laurin, G.V., Balling, J., Corona, P., Mattioli, W., Papale, D., Puletti, N., 2018. Above-ground Biomass Prediction by Sentinel-1 Multitemporal Data in Central Italy with Integration of ALOS2 and Sentinel-2 Data 12. <https://doi.org/10.1117/1.JRS.12>.
- Laurin, G.V., Puletti, N., Hawthorne, W., Liesenberg, V., Corona, P., Papale, D., Chen, Q., Valentini, R., 2016. Discrimination of tropical forest types, dominant species, and mapping of functional guilds by hyperspectral and simulated multispectral Sentinel-2 data. *Remote Sens. Environ.* 176, 163–176.
- Le Toan, T., Beaudoin, A., Riou, J., Guyon, D., 1992. Relating forest biomass to SAR data. *IEEE Trans. Geosci. Remote Sens.* 30, 403–411.
- Lee, J.-S., Pottier, E., 2009. Polarimetric Radar Imaging: from Basics to Applications. CRC press.
- Leemhuis, C., Jung, G., Kasei, R., Liebe, J., 2009. The Volta Basin Water Allocation System: assessing the impact of small-scale reservoir development on the water resources of the Volta basin , West Africa. *Adv. Geosci.* 21, 57–62.
- Lindsell, J.A., Klopf, E., 2013. Spatial and temporal variation of carbon stocks in a lowland tropical forest in West Africa. *For. Ecol. Manage.* 289, 10–17. <https://doi.org/10.1016/j.foreco.2012.09.045>.
- Louis, J., Debaecker, V., Pfugl, B., Main-Korn, M., Bieniarz, J., Mueller-Wilm, U., Cadau, E., Gascon, F., 2016. Sentinel-2 Sen2Cor: L2A processor for users. *Living Planet Symposium* 91.
- Lukin, V., Rubel, O., Kozhemiakin, R., Abramov, S., Shelestov, A., Lavreniuk, M., Meretsky, M., Vozel, B., Chehdi, K., 2018. Despeckling of multitemporal sentinel SAR images and its impact on agricultural area classification. *Recent Advances and Applications in Remote Sensing* 21–40 (IntechOpen).
- Lund, J.F., Sungusia, E., Mabele, M.B., Scheba, A., 2017. Promising change, delivering continuity: REDD+ as conservation fad. *World Dev.* 89, 124–139.
- Lung, M., Espira, A., 2015. The influence of stand variables and human use on biomass and carbon stocks of a transitional African forest: implications for forest carbon projects. *For. Ecol. Manage.* 351, 36–46.
- Malenovský, Z., Rott, H., Cihlar, J., Schaeppman, M.E., García-Santos, G., Fernandes, R., 2012. Sentinels for science: potential of Sentinel-1, -2, and -3 missions for scientific observations of ocean, cryosphere, and land. *Remote Sens. Environ.* 120, 91–101. <https://doi.org/10.1016/j.rse.2011.09.026>.
- Mermoz, S., Réjou-Méchain, M., Villard, L., Le Toan, T., Rossi, V., Gourlet-Fleurie, S., 2015. Decrease of L-band SAR backscatter with biomass of dense forest. *Remote Sensing of Environment* 159, 307–317.
- Moreno, J., Johannessen, J.A., Levelt, P.F., Hanssen, R.F., 2012. ESA's sentinel missions in support of Earth system science. *Remote Sens. Environ.* 120, 84–90. <https://doi.org/10.1016/j.rse.2011.07.023>.
- Müller, A., Weigel, J., Götz, A., Schmidt, O., Alva, I.L., Matuschke, I., Ehling, U., Beringer, T., 2015. The Role of Biomass in the Sustainable Development Goals: A Reality Check and Governance Implications, IASS WorkINg pAper. Potsdam: Institute for Advanced Sustainability Studies (IASS), Postdam.
- Mundava, C., Helmholtz, P., Schut, T., Corner, R., McAtee, B., Lamb, D., 2014. Evaluation of vegetation indices for rangeland biomass estimation in the Kimberley area of Western Australia. *Int. Arch. Photogramm. Remote Sens. Spat. Inf. Sci.* II-7, 47–53.
- Mutanga, O., Skidmore, A.K., 2004. Narrow band vegetation indices overcome the saturation problem in biomass estimation. *Int. J. Remote Sens.* 25, 3999–4014.
- Naidoo, L., Mathieu, R., Main, R., Wessels, K., Asner, G.P., 2016. L-band Synthetic Aperture Radar imagery performs better than optical datasets at retrieving woody fractional cover in deciduous, dry savannahs. *Int. J. Appl. Earth Obs. Geoinf.* 52, 54–64.
- Navarro, J.A., Algeet, N., Fernández-Landa, A., Esteban, J., Rodríguez-Noriega, P., Guillén-Climent, M.L., 2019. Integration of UAV, sentinel-1, and sentinel-2 data for mangrove plantation aboveground biomass monitoring in Senegal. *Remote Sens.* 11, 77. <https://doi.org/10.3390/rs11010077>.
- Nguyen, L.V., Tateishi, R., Nguyen, H.T., Sharma, R.C., To, T.T., Le, S.M., 2016. Estimation of tropical forest structural characteristics using ALOS-2 SAR data. *Adv. Rem. Sens.* 5, 131.
- Nicholson, S.E., Palao, I.M., 1993. A re-evaluation of rainfall variability in the sahel. Part I. Characteristics of rainfall fluctuations. *Int. J. Climatol.* 13, 371–389. <https://doi.org/10.1002/joc.3370130403>.
- O'neill, A.L., 1996. Satellite-derived vegetation indices applied to semi-arid shrublands in Australia. *Aust. Geogr.* 27, 185–199.
- Ouedraogo, A., Kakai, R.G., Thiombiano, A., 2013. Population structure of the wide-spread species, *Anogeissus leiocarpa* (DC.) Guill. & Perr. across the climatic gradient in West Africa semi-arid area. *South Afr. J. Bot.* 88, 286–295. <https://doi.org/10.1016/j.sajb.2013.07.029>.
- Pandit, S., Tsuyuki, S., Dube, T., 2018. Estimating above-ground biomass in sub-tropical buffer zone community forests, Nepal, using Sentinel 2 data. *Remote Sens.* 10, <https://doi.org/10.3390/rs10040601>.
- Pulliainen, J.T., Kurvonen, L., Hallikainen, M.T., 1999. Multitemporal behavior of L-and C-band SAR observations of boreal forests. *IEEE Trans. Geosci. Remote Sens.* 37, 927–937.
- R Core Team, 2017. R: A Language and Environment for Statistical Computing.
- Réjou-Méchain, M., Tanguy, A., Piponiot, C., Chave, J., Héraut, B., 2017. biomass: an R package for estimating above-ground biomass and its uncertainty in tropical forests. *Methods Ecol. Evol.* 8, 1163–1167.
- Rouse, J.W., Haas, R.H., Schell, J.A., Deering, D.W., 1974. Monitoring Vegetation Systems in the Great Plains with ERTS. In Proceedings, 3rd Earth Resources Satellite-1 Symposium 1, 309–317.
- Saatchi, S.S., Harris, N.L., Brown, S., Lefsky, M., Mitchard, E.T.A., Salas, W., Zutta, B.R., Buermann, W., Lewis, S.L., Hagen, S., Petrova, S., White, L., Silman, M., Morel, A., 2011. Benchmark map of forest carbon stocks in tropical regions across three continents. *Proc. Natl. Acad. Sci. U.S.A.* 108, 9899–9904. <https://doi.org/10.1073/pnas.1019576108>.
- Sanfo, S., 2010. Politiques publiques agricoles et lutte contre la pauvreté au Burkina Faso: le cas de la région du Plateau Central. Paris. pp. 1.
- Santoro, M., Beer, C., Cartus, O., Schmullius, C., Shvidenko, A., McCallum, I., Wegmüller, U., Wiesmann, A., 2011. Retrieval of growing stock volume in boreal forest using hyper-temporal series of Envisat ASAR ScanSAR backscatter measurements. *Remote Sens. Environ.* 115, 490–507. <https://doi.org/10.1016/j.rse.2010.09.018>.
- Santoro, M., Cartus, O., Fransson, J.E.S., Shvidenko, A., McCallum, I., Hall, R.J., Beaudoin, A., Beer, C., Schmullius, C., 2013. Estimates of Forest Growing Stock Volume for Sweden, Central Siberia, and Québec Using Envisat Advanced Synthetic Aperture Radar Backscatter Data. pp. 4503–4532. <https://doi.org/10.3390/rs5094503>.
- Schapire, R.E., Freund, Y., Bartlett, P., Lee, W.S., 1998. Boosting the margin: a new explanation for the effectiveness of voting methods. *Ann. Stat.* 26, 1651–1686. <https://doi.org/10.2307/120016>.
- Simons, H., Soto, X., Zhu, Z., Singh, K.D., Bellan, M.-F., Iremonger, S., Hirvonen, H., Smith, B., Watson, V., Tosi, J., others, 2001. Global Ecological Zoning for the Global Forest Resources Assessment 2000-Final Report.
- Sinha, S., Jegannathan, C., Sharma, L.K., Nathawat, M.S., 2015. A review of radar remote sensing for biomass estimation. *Int. J. Environ. Sci. Technol.* 12, 1779–1792.
- Sissoko, K., van Keulen, H., Verhagen, J., Tekken, V., Battaglini, A., 2011. Agriculture, livelihoods and climate change in the west african sahel. *Reg. Environ. Chang.* 11, 119–125.
- Skutsch, M.M., Ba, L., 2010. Crediting carbon in dry forests: the potential for community forest management in West Africa. *For. For. Policy Econ.* 12, 264–270. <https://doi.org/10.1016/j.forpol.2009.12.003>.
- Small, D., Schubert, A., 2008. Guide to ASAR Geocoding. *ESA-ESRIN Tech. vol. 36 Note RSL-ASAR-GC-AD*.
- Statnikov, A., Wang, L., Aliferis, C.F., 2008. A comprehensive comparison of random forests and support vector machines for microarray-based cancer classification. *BMC Bioinf.* 9, 319. <https://doi.org/10.1186/1471-2105-9-319>.
- Sylla, M.B., Giorgi, F., Pal, J.S., Gibba, P., Kebe, I., Nikema, M., 2015. Projected changes in the annual cycle of high-intensity precipitation events over West Africa for the late twenty-first century. *J. Clim.* 28, 6475–6488. <https://doi.org/10.1175/JCLI-D-14-00854.1>.
- Thenkabail, P.S., Ward, A.D., Lyon, J.G., Merry, C.J., 1994. Thematic Mapper vegetation indices for determining soybean and corn growth parameters. *Photogramm. Eng. Remote Sens.* 60, 437–442.
- Thiombiano, A., Glèlè-Kakai, R., Bayen, P., Boussim, J.I., Mahamane, A., 2015. Méthodes et dispositifs d'inventaires forestiers en Afrique de l'Ouest: état des lieux et propositions pour une harmonisation. *Ann. des Sci. Agron.* 19, 15–31.
- Torres, R., Snoeijs, P., Geudtner, D., Bibby, D., Davidson, M., Attema, E., Potin, P., Rommen, B., Flory, N., Brown, M., Traver, I.N., Deghaye, P., Duesmann, B., Rosich, B., Miranda, N., Bruno, C., L'Abbate, M., Croci, R., Pietropolo, A., Huchler, M., Rostan, F., 2012. GMES Sentinel-1 mission. *Remote Sens. Environ.* 120, 9–24. <https://doi.org/10.1016/j.rse.2011.05.028>.
- UNEP/CBD/SBSTTA, 2016. Framework and Guiding Principles for a Land Degradation Indicator. (Montreal, Canada).
- UNSD, 2019. E-handbook on sustainable development goals indicators. [WWW Document]. URL <https://unsd.un.org/wiki/display/SDGeHandbook/Home?preview=/34505092/38535788/SDGeHandbook-150219.pdf>.
- Vafaei, S., Soosani, J., Adeli, K., Fadaei, H., Naghavi, H., Pham, T.D., Bui, D.T., 2018. Improving accuracy estimation of Forest Aboveground Biomass based on incorporation of ALOS-2 PALSAR-2 and Sentinel-2A imagery and machine learning: a case study of the Hyrcanian forest area (Iran). *Remote Sens.* 10. <https://doi.org/10.3390/rs10020172>.
- Vaglio Laurin, G., Liesenberg, V., Chen, Q., Guerriero, L., Del Frate, F., Bartolini, A., Coomes, D., Wilebore, B., Lindsell, J., Valentini, R., 2013. Optical and SAR sensor synergies for forest and land cover mapping in a tropical site in West Africa. *Int. J. Appl. Earth Obs. Geoinf.* 21, 7–16. <https://doi.org/10.1016/j.jag.2012.08.002>.
- Wählinder, A., 2014. Evaluation of Logistic Regression and Random Forest Classification Based on Prediction Accuracy and Metadata Analysis.
- Way, J., Paris, J., Kaschick, E., Slaughter, C., Viereck, L., Christensen, N., Dobson, M.C., Ulaby, F., Richards, J., Milne, A., others, 1990. The effect of changing environmental conditions on microwave signatures of forest ecosystems: preliminary results of the March 1988 Alaskan aircraft SAR experiment. *Int. J. Remote Sens.* 11, 1119–1144.
- Weber, J.C., Montes, C.S., Abasse, T., Sanquette, C.R., Silva, D.A., Mayer, S., Muniz,

- G.I.B., Garcia, R.A., 2018. Variation in growth, wood density and carbon concentration in five tree and shrub species in Niger. *New Times* 49, 35–51.
- Weiss, M., Baret, F., 2016. S2ToolBox Level 2 Products: LAI, FAPAR, FCOVER. INRA, EmmaH. CAPTE.
- White, F., 1986. La Végétation de l'Afrique-Recherches Sur Les Ressources Naturelles. ORSTOM - UNESCO, Paris.
- Wingate, V., Wingate, V.R., Phinn, S.R., Kuhn, N., Scarth, P., Wingate, V.R., Phinn, S.R., Kuhn, N., Scarth, P., 2018. Estimating aboveground woody biomass change in Kalahari woodland: combining field, radar, and optical data sets. *Estimating aboveground woody biomass change in Kalahari woodland: combining field, radar, and optical data sets. Int. J. Remote Sens.* 39, 577–606. <https://doi.org/10.1080/01431161.2017.1390271>.
- Yilma, T., 2006. Modeling Farm Irrigation Decisions under Rainfall Risk in the White Volta Basin of Ghana. A Tool for Policy Analysis at the Farm-household Level. University of Göttingen, Göttingen.
- Zanne, A.E., Lopez-Gonzalez, G., Coomes, D.A., Ilic, J., Jansen, S., Lewis, S.L., Miller, R.B., Swenson, N.G., Wiemann, M.C., Chave, J., 2009. Global Wood Density Database.
- Zeidler, J., Wegmann, M., Dech, S., 2012. Spatio-temporal robustness of fractional cover upscaling: a case study in semi-arid Savannah's of Namibia and Western Zambia. In: *Earth Resources and Environmental Remote Sensing/GIS Applications III*, pp. 85380S.
- Zhang, H., Li, Q., Liu, J., Shang, J., Du, X., McNairn, H., Champagne, C., Dong, T., Liu, M., 2017. Image classification using rapideye data: integration of spectral and textual features in a random forest classifier. *IEEE J. Sel. Top. Appl. Earth Obs. Remote Sens.* 10, 5334–5349.
- Zhao, P., Lu, D., Wang, G., Liu, L., Li, D., Zhu, J., Yu, S., 2016. Forest aboveground biomass estimation in Zhejiang Province using the integration of Landsat TM and ALOS PALSAR data. *Int. J. Appl. Earth Obs. Geoinf.* 53, 1–15.
- Zoungrana, B.J.B., Conrad, C., Thiel, M., Amekudzi, L.K., Da, E.D., 2018. MODIS NDVI trends and fractional land cover change for improved assessments of vegetation degradation in Burkina Faso, West Africa. *J. Arid Environ.* 153, 66–75.